fibers

MDPI

Review

Advancements in Design and Manufacture of High-Performance Modified Carbon/Carbon Composites for Extreme Aerospace Environments: A Comprehensive Review

Johnson I. Humphrey [1], Stephen Dobreh [2], Md Mostafizur Rahman [3], Ayomide Sijuade [1] and Okenwa I. Okoli [1,*]

[1] Department of Mechanical Engineering, Herff College of Engineering, The University of Memphis, Memphis, TN 38152, USA; jhmphry7@memphis.edu (J.I.H.); asijuade@memphis.edu (A.S.)
[2] Department of Mechanical Engineering, College of Sciences and Engineering, Southern University and A&M College, Baton Rouge, LA 70813, USA
[3] Department of Chemical Engineering and Polymer Science, Shahjalal University of Science and Technology, Sylhet 3114, Bangladesh
* Correspondence: o.okoli@memphis.edu

Abstract

The demand for materials that can operate reliably in extreme environments, including rocket nozzles, re-entry heat shields, sharp leading edges, high-velocity impact, and high-temperature energy systems, continue to drive advances in thermal–structural materials. Carbon/Carbon composites remain a leading baseline because of their low density, high-temperature mechanical retention in inert atmospheres, and excellent thermal-shock tolerance. However, long-term durability is constrained by rapid oxidation in air at elevated temperatures, limited fracture toughness and elastic modulus in many architectures, and high manufacturing cost driven by multi-cycle densification and stringent quality assurance. Consequently, contemporary strategies increasingly rely on modifying Carbon/Carbon composites with ultra-high-temperature ceramics and adopting accelerated or simplified manufacturing routes. This review synthesizes recent progress in the design, manufacture, and application of high-performance modified Carbon/Carbon composite systems for extreme aerospace environments, emphasizing composition/architecture selection, oxidation, and ablation protection, toughening concepts, and cost-aware densification. Because extreme environments performance is governed by coupled aerothermal loading, gas–surface chemistry, internal transport, recession, and thermomechanical response, the review also consolidates the multiscale modeling and software toolchains increasingly used to size thermal-protection systems, interpret experiments, and guide down-selection. Key challenges and future directions are further discussed for reusable materials and validated performances beyond ~2000 °C.

Keywords: ultra-high-temperature ceramic matrix composites; ultra-high-temperature ceramics; Carbon/Carbon composites; extreme environments

Academic Editor: Catalin R. Picu

Received: 20 December 2025
Revised: 15 April 2026
Accepted: 28 April 2026
Published: 8 May 2026

1. Introduction

The development of advanced materials capable of sustaining extreme environments (EEs) is a critical challenge in modern aerospace engineering. These environments are characterized by severe thermochemical and mechanical loads, including temperatures exceeding 1500–3000 °C, high heat fluxes (>100–1000 W/cm^2), oxidative and ablative conditions, and rapid thermal cycling during hypersonic flight and atmospheric re-entry [1–4].

Such conditions impose stringent requirements on structural integrity, thermal stability, oxidation resistance, and damage tolerance [5,6].

In this context, Carbon/Carbon composites (C/CCs), which consist of carbon fibers reinforced within a carbon matrix, remain prime candidates for hot-structure and thermal protection system (TPS) sub-elements because of their high specific stiffness and strength, low coefficient of thermal expansion (CTE), and excellent thermal-shock tolerance at temperatures where metals and many ceramics fail (with the critical caveat that bare C/CCs require oxidation protection in air) [1]. Contemporary reviews and NASA practice underscore two complementary TPS pathways: (i) carbon-based ablators and woven carbon-phenolics for entry systems (e.g., Phenolic Impregnated Carbon Ablator (PICA), Heatshield for Extreme Entry Environment Technology (HEEET), 3D Mid-Density Carbon Phenolic (3MDCP), and 3D Multifunctional Ablative TPS (3D-MAT) [7–10]), and (ii) structural C/C upgraded via ultra-high-temperature ceramics (UHTCs) or high entropy ceramics (HECs) additives or coatings to resist oxidation and ablation under extreme heat flux [4,5,11]. C/CCs (often coated or modified) have long been a TPS mainstay for the highest heat loads. The Space Shuttle's reinforced carbon-carbon (RCC) was a C/CC reinforced with carbon fibers and reacted with silicon to form a C/C–SiC structure [12]. These low-density, high-temperature structural materials can withstand ∼1400–1650 °C, far beyond what aluminum or silica tiles endure [12]. However, unprotected C/CCs oxidize rapidly in air above ~500 °C [1]. Even with coatings, any breach can lead to burn-through. At the same time, the limited use of carbon-fiber (CF) fabrics and CF prepregs in industrial parts is also driven primarily by cost, and by production speed or scale, certification and repair challenges, recyclability, and prepreg handling constraints [13–15]. This also translates to C/CCs, with TPS being expensive to fabricate and becom quasi-brittle under mechanical stress [16]. Therefore, it is essential to develop C/CC-based TPS that meet extreme aerospace environment requirements while remaining lightweight and manufacturable through cost-effective, scalable, and environmentally safe processing routes [17–19]. Table 1 shows the comparison of the state-of-the-art TPS as well as their advantages and disadvantages. It represents a significant step towards reusable heat shields; however, material constraints and limited flight heritage remain key challenges. Reusable TPS today are limited to silica-based tiles that tolerate about 1200–1260 °C with good thermal-shock resistance but become brittle and crack at higher heat loads [20]. This prevents truly reusable orbital systems from reaching the 2000 °C regime. Newer hybrids like the Toughened Uni-piece Fibrous Reinforced Oxidation-Resistant Composite (TUFROC) stretch reusability toward (~1590 °C), but, beyond that, the design starts to look like a single-use one again [21]. Reaching higher, the Shuttle-era RCC proved that load-bearing hot structures can ride through a ~1650 °C reentry as long as their SiC skin remains pristine [20]. And, when missions truly survive above ~2000 °C, we still pay in terms of consumed thickness (mass loss), rather than through refurbishment, while using ablatives like PICA, HEEET, and 3D-woven systems that char and erode by design.

UHTCs and HECs offer a pathway for usage as sharp leading edges past 2000 °C without ablation due to entropy-stabilized lattices and more resilient oxide chemistry, but brittleness, joints, and oxidation under real entry flows remain challenging, i.e., a material that is strong in a furnace can still crack at very high Mach numbers, and an oxide scale that protects in a lab can spall in flight.

Table 1. Comparison of the state-of-the-art TPS for EEs.

TPS	Composition	Peak Capability	Reusability	Advantages	Disadvantages	References
(SIRCA)	Silicone resin-impregnated rigid ceramic fiber substrate (silica-based)	Used in low–moderate heating $\leq$ ~100 W/cm^2.	No	Flight heritage, easily machined, good insulator.	Lower heat-flux envelope vs. high-capability ablators.	[22]
PICA	Phenolic resin-impregnated Ablator (FiberForm substrate)	Cold-wall peak heating up to ~1200 W/cm^2 class; widely used on Stardust, Dragon.	No	Very mass-efficient at high heat flux; broad flight heritage.	Brittle: tiled integration for large diameters adds seams/gaps.	[9]
3D-MAT	3D woven quartz fiber/cyanate ester composite with ablative matrix	Qualified for Orion Earth-return wedge/compression-pad environments (arc-jet tested; superior insulation vs. carbon-phenolic).	No	Tailorable 3D weave; structural + ablative; better insulation than carbon-phenolic for pad duty.	Niche application (pad region), not acreage.	[8]
HEEET	Dual-layer 3D woven carbon/insulating layer tiles	Tested to ~6500 W/cm^2, ~5.5 atm; Venus/Saturn-class entries.	No	Very high heat-flux/pressure capability.	Newer supply chain; tiled integration complexity.	[10,23]
3MDCP	Carbon fiber-reinforced phenolic resin matrix composite	Very high-enthalpy/pressure regimes (carbon-phenolic class).	No	Extreme environment capability; carbon-phenolic heritage.	High density (mass penalty); material sustainability/supply issues historically.	[24]
Shuttle LI-900/LI-2200)	High-temperature Reusable Surface Insulation (HRSI): Silica fiber tiles with Reaction-Cured Glass (RCG) coating	Multi-use (1260–1480 °C).	Yes	Ultra-low density & conductivity; 100-flight heritage.	Impact-sensitive; labor-intensive inspection/repair.	[20]
Fibrous Refractory Composite Insulation (FRCI) or Alumina-Enhanced Thermal Barrier (AETB)	AETB composite fiber tile substrate with Toughened Uni-piece Fibrous Insulation (TUFI) or RCG surface coatings	AETB: up to ~2800 °F (1538 °C) single-use; HRSI-class multi-use ~2300–2600 °F.	Yes	Better strength/durability vs. pure silica tiles; modernized tile baseline.	Still seam/gap system; coating processing adds cost.	[20]
TUFROC	Bi-layer system: oxidation-resistant carbonaceous cap bonded to low-density fibrous refractory insulation substrate	Reusable ~2900 °F (≈1590 °C); single-use >3100 °F (≈1700 °C).	Yes	Lightweight, insulative, oxidation-resistant leading edge option; cheaper than C/C.	Limited to leading edge duty; still tiled interfaces.	[21]
Starship ceramic tiles	Ceramic hexagonal tiles on stainless steel acreage; details proprietary	Public numeric limits not disclosed.	Yes	Reusable acreage tiling on metallic structure; rapid turn-around goal.	Tile durability/attachment challenges; limited open data.	
New Shepard TPS	Suborbital crew capsule with reusable TPS (details not public)	Suborbital entries, milder heating than orbital; TPS suited to reusable regimes.	Yes	Multiple flights with minor refurbishment.	Specific materials/limits undisclosed.	[25]
RCC	Carbon–carbon with SiC/oxide conversion coating	~3000–3220 °F (≈1650–1770 °C) service.	Yes	Carries load (“hot structure”), very high temperature.	Oxidation/impact vulnerability; coating integrity critical.	[20]
UHTCs	Refractory monoborides, carbides, or nitrides of Hf, Zr, or Ta	>2000 °C oxidation-resistant service (composition & atmosphere dependent.	Potentially as hot structure	Very high melting points, good thermal conductivity; candidate for sharp edges.	Oxidation management at lower T for carbides; processing complexity.	[26]
HECs	Multi-principal carbides/borides/nitrides	Lab results indicate high-T stability (>1800–2000 °C); active research.	Ongoing Research	Tunable properties; promising oxidation & creep behavior.	Early stage; limited flight heritage.	[27]

Table 1. *Cont.*

TPS	Composition	Peak Capability	Reusability	Advantages	Disadvantages	References
Ultra-High-Temperature Ceramic Matrix Composites (UHTCMCs)	Continuous carbon-fiber reinforced ZrB_2–SiC or HfB_2–SiC matrices	Arc-jet exposures of Cf/ZrB_2–SiC bars up to ~2200 °C (~2 min).	Potentially reusable hot structure	Combines high-T capability of UHTCs with composite toughness; better damage tolerance than monolithic UHTCs.	Oxidation/volatilization management required; processing complexity.	[28,29]
HEC-modified C/CCs	C/CCs substrate with high-entropy ceramic coatings or matrix modifications comprising multi-principal carbides (HECCs), borides (HEBs), nitrides (HENs), or oxides (HEOs)	Entropy-stabilized diboride coatings on carbon tested for ablation up to ~2200 °C.	Potentially reusable hot structure	Tailorable oxide-scale chemistry and entropy-stabilized single-phase behavior can slow oxidation and ablation.	Maturity/scale-up: long-duration, cyclic oxygen-rich exposures and thermal-gradient durability data are still building.	[30]

So, at present, reusable heat shields are generally limited to surface temperatures below ~1600 °C, whereas environments approaching and exceeding ~2000 °C are typically addressed using ablative protection. This division reflects not a lack of ambition, but the temperature and oxidation limits that current state-of-the-art materials can reliably withstand. So, it is imperative to design and develop high-performance TPS that can be reused above ~2000 °C by combining oxidation-resistant, damage-tolerant surface architectures, robust matrices, and in situ inspection over low-mass insulating substructures, thereby bridging the current performance gap between tiles reusable below ~1600 °C, ~1650 °C hot structures, and >2000 °C single-use ablators.

Figure 1 depicts potential TPS solutions for extreme aerospace environments: mapping fracture toughness vs. elastic modulus. Figure 1 clearly illustrates how HECs, especially High-Entropy Carbide Ceramics (HECCs) among others, as modifiers to C/CCs, can play a role in developing next-generation TPS.

Although still in the early research and developmental stage, HECCs, compared to other monolithic UHTCs and HECs, offer a compelling synergy between fracture toughness (~15 MPa·$\sqrt{m}$) and high elastic modulus (~450–550 GPa), which is critical for maintaining structural integrity under hypersonic and thermal shock environments. As shown, HECCs are among the few systems approaching a key projected performance goal for extreme aerospace applications and thus could justify their selection for further C/CC modification. However, these projections are primarily based on laboratory-scale data, and validation under coupled aerothermal environments remains limited. Figure 2 shows the evolution and vision of composites trailing toward embedded sensor-modified C/CCs. Details of the design and manufacturing methods for these materials are discussed in Section 3.

While numerous studies have investigated UHTC-based materials, C/CCs, or TPS individually, these topics are often treated separately in literature. However, the development of ceramic-modified C/CCs for extreme aerospace environments requires simultaneous consideration of material selection parameters, manufacturing feasibility, and predictive modeling tools, particularly in the context of reusable TPS design. Integrating these perspectives remains an important challenge for advancing next-generation TPS. Accordingly, this review evaluates current design strategies and modification architectures that retain C/CCs as the structural substrate while enhancing their performance through surface and matrix modifications. These include SiC-based variants, UHTC coatings, subsurface damage-tolerant modifiers, and emerging UHTCMC systems, with particular emphasis on their potential to enable reusable TPS that could operate beyond the ~2000 °C regime.

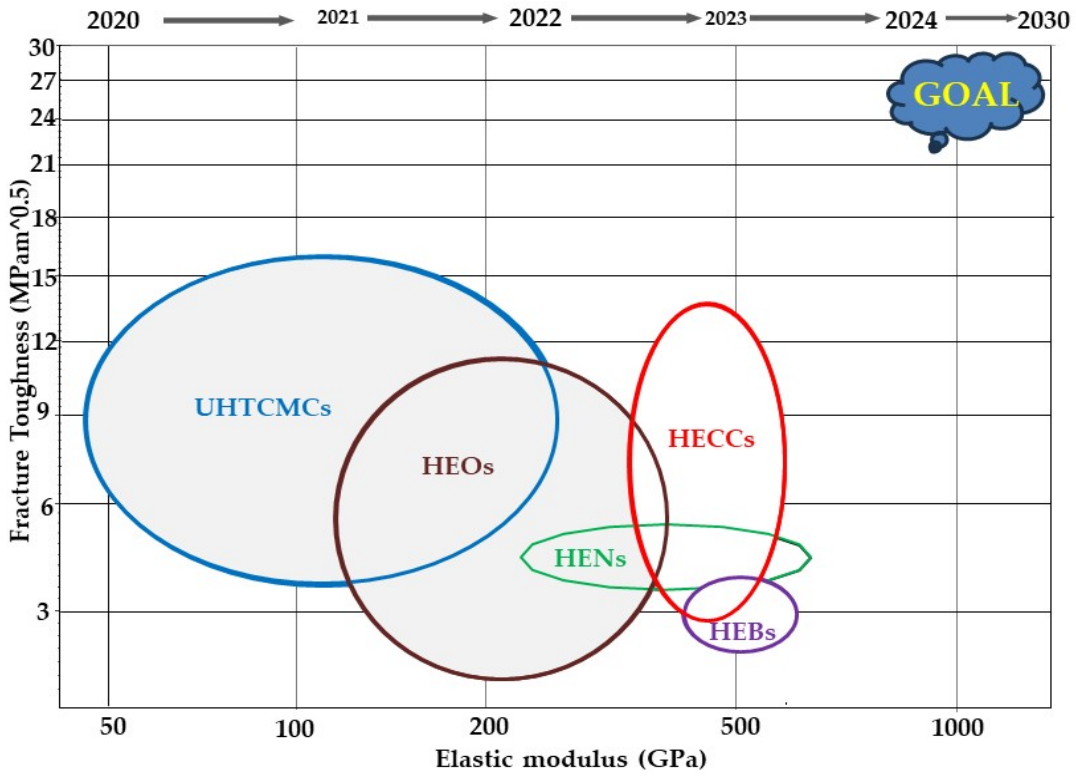

Figure 1. Fracture toughness vs. elastic modulus material properties and roadmap on High Entropy Carbide Ceramics (HECCs) [31–34], High Entropy Oxides (HEOs) [35–38], High Entropy Nitrides (HENs) [39–42], High Entropy Borides (HEBs) [43–46], and UHTCMCs [47–50] materials for EEs.

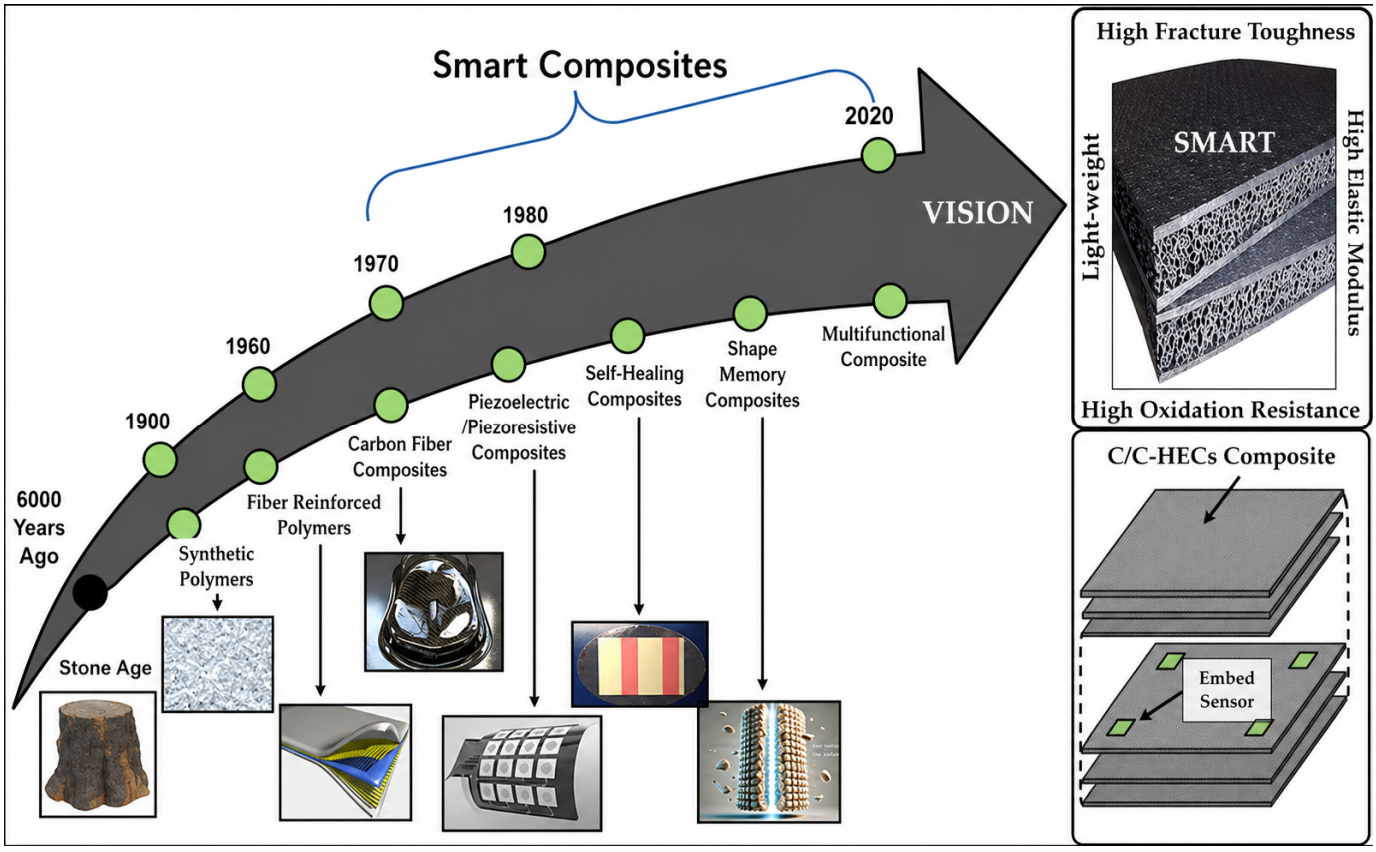

Figure 2. Evolution/innovation in composites and the vision toward materials for EEs.

2. Materials for EEs: Modified C/CC Systems and Related UHTCMCs

Modified C/CCs refer broadly to C/C architectures whose baseline C/C (carbon fiber and carbon matrix) is enhanced for extreme environments using coatings, dopants, near-surface conversion, or infiltrated ceramic phases (e.g., UHTC matrix). By contrast, UHTCMCs denote continuous-fiber-reinforced ultra-high-temperature ceramic matrix composites. Here, the reinforcement may be carbon fiber embedded in a UHTC matrix (carbide/boride/nitride-based) to improve damage tolerance relative to monolithic UHTCs. Accordingly, the two terms are overlapping but not equivalent: many modified C/CCs remain fundamentally C/C with added protective phases, whereas UHTCMCs represent cases where a UHTC-rich matrix plays a dominant structural role [51]. Table 2 highlights the fundamental trade-offs between oxidation resistance, mechanical integrity, and density. While UHTCs exhibit superior thermal stability, their low fracture toughness limits structural use, whereas C/CCs offer excellent toughness but require oxidation protection. Hybrid systems such as UHTCMCs aim to balance these competing requirements but introduce processing and cost challenges.

Table 2. Comparative thermomechanical and environmental performances of candidate materials for thermal protection systems (TPS) in extreme environments.

Material System	Max Service Temp (°C)	Thermal Conductivity (W/m·K)	Fracture Toughness (Mpa.m$^{1/2}$)	Density (g/cm^3)	Oxidation Resistance	Key Limitation	References
C/C	~2000 (inert)	4–35	10–20	1.6–1.9	Poor (>500 °C in air)	Oxidation vulnerability	[1,52]
C/C–SiC (RCC-type)	~1600–1700	5–20	8–15	1.8–2.2	Moderate	Coating damage sensitivity	[12,53]
UHTCs (e.g., ZrC, HfC)	>2500–3000	10–30	2–5	6–12	Excellent	Brittleness	[4,54]
UHTCMCs	~2000–2200	5–25	10–20	2.5–3.5	Good	Processing complexity	[50]
HECs	~1800–2200 *	Variable	3–8 *	6–10	Promising	Limited validation	[34]
Ablative TPS (e.g., PICA)	>2000 (transient)	Low	N/A	0.25–0.9	Excellent (sacrificial)	Single-use	[9,55]

* Values vary widely depending on composition and maturity of system.

Table 2 shows that C/C remains the preferred structural core across all architecture due to its unmatched toughness-to-density ratio but requires surface protection above 500 °C in oxidizing environments. C/C–SiC is the logical choice for reusable hot structures up to ~1700 °C but, beyond this limit, UHTC coatings or UHTCMCs become necessary despite their higher processing complexity and density. Monolithic UHTCs should not be used as standalone load-bearing materials due to their low fracture toughness and are better applied as surface coatings or conversion layers on a C/C substrate. HECs show promise as oxidation-resistant phases but currently lack sufficient validation under flight-relevant conditions, limiting their use to experimental surface modifiers. Ablative TPS remains the most mass-efficient solution for high heat flux, single-entry missions where reusability is not required. Overall, no single system satisfies all performance criteria simultaneously, reinforcing the need for hybrid modified C/C architectures, as discussed in the following sections.

2.1. UHTC-Modified C/CC Systems (C/C–UHTCs) and C/C-Derived UHTCMCs

Traditionally, single-piece C/CCs have been commonly acknowledged as the key base material for designing and manufacturing hypersonic leading edges, as depicted in Figure 3.

This reputation stems from their exceptional characteristics, including their low density (1.60–1.98 g/cm^3), low thermal expansion (-0.85 to 1.1 $\times$ 10^{-6}/K), high elasticity modulus (200 GPa), impressive thermal conductivities (~4–35 W/mK), and the capability to sustain their mechanical properties up to around 2000 °C in inert atmospheres [2,52,56]. Despite the remarkable properties of C/CCs, they begin to oxidize at a relatively low temperature of approximately 370 °C in air, and experience significant oxidation above 500 °C [1].

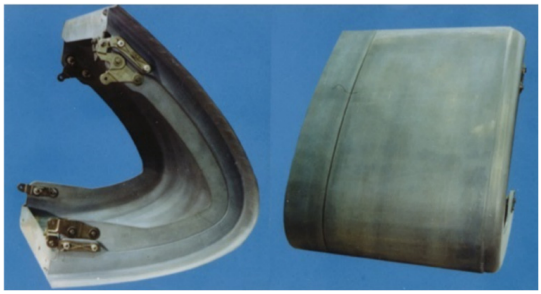

Figure 3. Space shuttle orbiter leading edge designed and manufactured with C/CCs [57].

Without protective measures against oxidation, using single-piece C/CCs in high-heat and oxidative conditions can lead to disastrous failures. This oxidation issue has significantly hindered the long-term and widespread application of C/CCs. As global demands for ultra-high-temperature materials increase, developing methods to shield C/CCs from intense heat-induced oxidation, material loss, and wear has become an urgent necessity [58–61]. Figure 4 illustrates the energy management mechanism in ablative and reusable Thermal Protection Materials (TPMs), essential for resisting oxidation, thermal stress, material removal, and wear due to gas flow at elevated temperatures. Figure 4a emphasizes chemical diffusion, mechanical erosion, and melt flow, highlighting the physical and chemical interactions that occur during thermal protection. Figure 4b focuses on the layered structure of thermal barrier coating and low conductivity insulation, emphasizing material properties and heat resistance. Generally, these diagrams collectively provide a comprehensive view of the TPS' functioning, illustrating the different layers and processes involved in protecting the structures from extreme heat conditions.

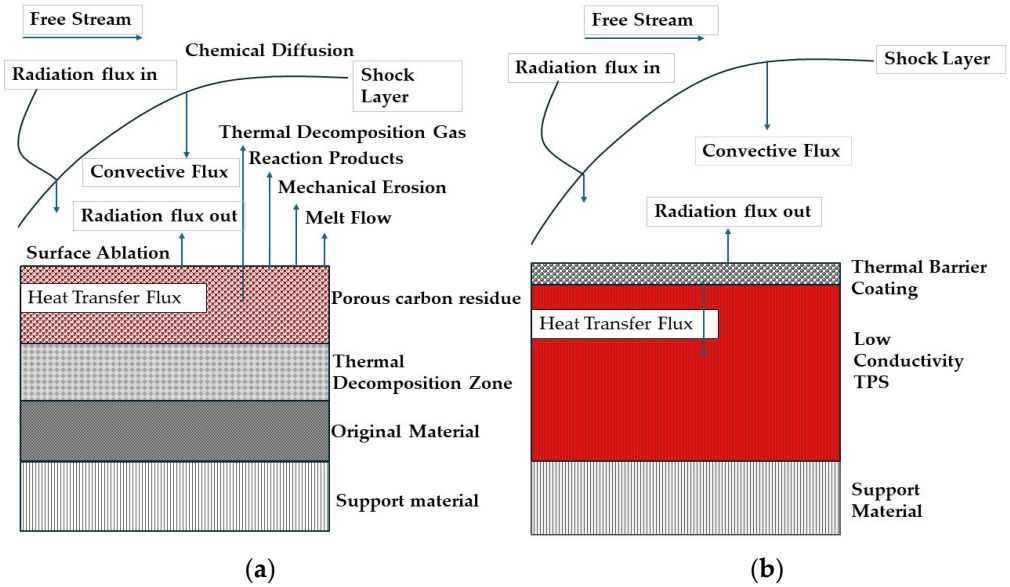

Figure 4. Energy accommodation process for (**a**) reusable TPMs and (**b**) ablative TPMs [22].

2.1.1. Weight Factors for Modified C/CCs

For aerospace TPS (including sharp leading edges), lightweight is most meaningfully evaluated as mass per protected area (TPS areal mass/areal density, kg/m^2), because TPS trade studies, as noted by the NASA HEET project, compare candidates after they have been sized for a common trajectory and heating environment (i.e., compare TPS areal mass for the same trajectory) [62]. Once the entry environment is established, material response modeling is used to determine the TPS thickness required to keep the bondline/backface temperature below a specified limit and to account for surface recession where applicable, which is why thickness and not density alone becomes the key bridge between material properties and mass [22].

Consistent with this practice, NASA sizing studies commonly report results in terms of areal density after thickness sizing; for example, Fully Implicit Ablation and Thermal response (FIAT)-based TPS sizing computations for aerocapture explicitly states size thickness as a function of heat load and then summarize outcomes "in terms of areal density," highlighting that the areal metric is the basis for comparing mass efficiency across TPS options [63].

Thickness is therefore the second, inseparable weight driver. NASA TPS sizing practice illustrates that thickness depends strongly on the integrated heat load and the allowable internal temperature limits; once thickness is set, mass is compared as areal density, and further savings can come from spatially tailoring thickness (variable-thickness sizing) rather than uniform layups [63]. This logic transfers directly to modified C/CC concepts because coatings and graded surface architectures may add mass locally, but if they suppress oxidation/recession or expand the usable temperature/pressure window, they can reduce the total "consumed thickness and margin thickness" that must be carried, hence improving net areal density. The X-43A leading edge material system is a useful illustration of how modified C/CCs are often engineered for mass efficiency: the design retained a high thermal conductivity, thermally biased C/C substrate and relied on a thin protective multilayer coating stack to extend oxidation/temperature capability without converting the entire volume to a denser ceramic composite. This is a weight-driven philosophy which preserves the low-density, high-specific-performance carbon architecture for the load-bearing bulk and places the mass-added functionality (environmental protection) where it is most leveraged (at the surface) [64]. By contrast, integrated UHTC/HEC-modified C/CC routes (e.g., particle impregnation into the preform followed by densification) move more of the ceramic mass into the volume, which can raise bulk density but can also improve oxidation resistance of the fibers and thermal-shock resistance at ultra-high temperatures. The correct way to judge whether such routes are *mass efficient* would be to report the resulting *sized* areal density for a given EE load case (including coating/substrate/adhesive/joint features where relevant), rather than inferring advantage from higher performance or disadvantage from "higher density" in isolation.

Density to areal density for modified C/CCs concepts (C/SiC, SiC-converted RCC, C/C-UHTC/HEC hybrids, UHTC/HEC coatings, graded stacks) matter because they change the weight factors in two competing ways:

a. **They often increase effective density** because added phases (e.g., SiC, ZrC–SiC, HfC/SiC coating layers) and reduced porosity raise mass per volume. For example, heritage RCC is valued for relatively low density (reported around ~1.6–1.8 g/cm^3 in a NASA overview), which is a key reason that it is historically attractive for leading edge hot structures [53]. However, modified versions frequently densify the near-surface or bulk. A representative UHTC-modified example reports C/C-ZrC-SiC density $\approx$ 2.74 g/cm^3 (with open porosity $\approx$ 8.6%), which is materially heavier per unit thickness than baseline C/C/RCC-class densities. Another clear example of

"bulk density is architecture and densification state" appears in the recent Reactive Melt Infiltration (RMI) work that produced thick, reusable, ceramic-modified carbon-based composites. Guo et al. [65] reported a 20 mm thick Cf/SiC–ZrC material (a C/CC-derived UHTCMC class) fabricated by RMI with a density of 2.79 $g \cdot cm^{-3}$ and open porosity of 5.65%, designed specifically to improve through-thickness integrity and transport while retaining load-bearing capability after ablation exposure. What matters for "mass efficiency" here is not that the material is denser than monolithic/bare/heritage C/CCs, but it is that the design target is reusable under high heat flux, where the allowable recession and retained mechanical margin can materially reduce the *sized* thickness (or reduce the number of sacrificial layers/allowances) needed to meet EE constraints.

b. **They can reduce the thickness that must be carried** (and/or reduce recession allowance), because improved oxidation and ablation resistance and higher temperature capability can reduce how much material is needed to survive the mission [55,66]. That is the central mass-efficiency trade where a heavier per mm stack can still be lighter per m^2 if the design is thinner for the same environment. NASA's aerocapture TPS sizing discussion captures this principle generally because material selection choice changes thickness, and the correct comparison is the resulting areal density after sizing [67].

At component/system level, the areal density of a modified C/CCs solution is best thought of as a stacked sum of the mass of the substrate, conversion layers, coatings, bondlines, and attachment penalties [68]. This breakdown is important because, for leading edges, the non-carbon additions are often not "free" in mass terms:

a. **Surface conversion/seal/coating mass** can be modest if coatings are thin, but it grows quickly if thickness is increased for durability/crack tolerance [69]. Several recent coating studies explicitly show the recession-rate leverage that drives thickness, areal density, and even coatings, add mass [70]. Junshuai et al. [71] reports a linear recession rate close to zero (~0.11 $\mu m \cdot s^{-1}$) after two 120 s ablation cycles, illustrating how a dense UHTC barrier can sharply suppress net material loss under repeated EE-relevant exposures. In the same direction, recent high-/medium-entropy ceramic coating studies emphasize that these multicomponent carbides/borides are being pursued precisely because their oxidation products and phase stability can outperform simpler monocarbides/monoborides at ultra-high temperatures, i.e., their role is to push the recession/oxidation boundary outward so the carbon-bearing structure does not have to "pay" for protection through extra thickness [72].

b. **Bulk densification route and porosity closure** are major weight drivers. If a modified route closes more porosity, density rises, which directly increases areal density for a fixed thickness [73]. The C/C-ZrC-SiC example above ($\approx$2.74 g/cm^3) is a clear demonstration that UHTC-containing modifications can push density well above baseline C/C/RCC-class values [64].

c. **Infiltration/modification depth matters.** In a thesis-focused study on modified C/C–SiC systems, adding β-SiC nanoparticles and producing a modified near-surface region (reported modification depth on the order of ~100 μm scale) increased near-surface density and altered oxidation behavior, which is exactly the kind of "small thickness, real areal-mass" effect designers/researchers must track and consider for material selection [74]. Crucially, multiple studies on ceramic modification via infiltration show that "weight" changes are inseparable from how much ceramic is introduced and where it ends up in the architecture [73,75–77]. Liu et al. [73] prepared a porous C/C preform and noted that the preform's porosity governs how much melt can be taken up during infiltration and explicitly remarks that this

plays an important role in increasing the density/weight of the modified composite. Therefore, the mass penalty is real and measurable, but it is only unfavorable if it does not translate into a larger reduction in required thickness (through lower recession, lower oxidation-driven knockdown, reduced uncertainty margins, or fewer protective sublayers).

d. **Geometry choices interact with weight.** Leading edge design often faces a geometry trade: blunting (larger radius) can reduce peak heating, but it can also penalize aerodynamic performance and can require more material volume (hence more mass) [78]. A recent ORNL technical chapter discussing X-43 materials explicitly frames the historical blunt vs. sharp leading-edge choice as a coupled aero–thermal–materials trade [53].

2.1.2. Thermal Conductivity Management in Modified C/CCs for EEs

Thermal conductivity in modified C/CCs should be treated as a design variable rather than a fixed material property, because oxidation-protection strategies (UHTC/SiC-based coatings, infiltrated carbides/borides, and nano/micro reinforcements) often change the heat-flow pathways and therefore the near-surface thermal gradients that control ablation, thermal shock damage, and coating integrity. For sharp leading edges, the classical rationale for C/CCs is not only high-temperature strength, but also the ability to conduct heat away from stagnation regions. The NASA thermal conductivity database emphasizes how widely C/CCs conductivity can vary (and thus be tailored) with architecture and processing [79]. Recent work reinforces that conductivity tailoring can be achieved by engineering the carbon network and then overlaying oxidation protection. For example, Li et al. [80] designed a 3D C/C architecture using high-conductivity pitch-based fibers in selected directions to achieve strongly anisotropic high thermal conductivity, illustrating a practical path to heat spreading while retaining carbon's low CTE advantage. In parallel, coating-centric studies show that heat-spreading within the protective layer itself can be decisive. In that regard, Zhang et al. [69] introduced a ceramic carbon core–shell concept (including a graphene/carbon shell) in a ZrC–SiC/TaC coating and explicitly framed the benefit as improved heat dissipation, which reduced surface temperature rise and helped suppress ablation-driven damage accumulation.

Therefore, in modified C/CCs, the best-performing oxidation and ablation solutions are unlikely to be insulating or conductive everywhere. Instead, they tend to preserve (or deliberately build) directional heat-spreading pathways in the carbon skeleton and/or the protective layer to lower peak temperatures and thermal gradients, while still maintaining adequate through-thickness insulation where the backface temperature limit governs design. The literature supports this co-optimization mindset where conductivity tailoring is feasible at the architecture level, and coating designs can be explicitly engineered to manage heat flow (not only oxygen diffusion) [80]. Many EE-driven modifications (SiC/UHTC/HEC phases, hybrid matrices, coatings) can unintentionally *reduce* effective conductivity or create thermal bottlenecks if they interrupt carbon heat-flow networks or introduce high-resistance interfaces. Zhao et al. [81] study on C/C–ZrC–SiC explicitly framed insufficient thermal conductivity as a practical limitation because it promotes surface heat accumulation during ultra-high-temperature exposure, and it proposes mesophase pitch-based carbon fibers as engineered heat-transfer channels to restore heat spreading while improving ablation resistance. This heat-channel logic is consistent with earlier ZrC–SiC-modified C/C demonstrations that intentionally use mesophase pitch fibers and pyrocarbon to create continuous thermal diffusion paths and report very high in-plane thermal conductivity to reduce ablation-driven thermal localization [82]. Wang et al. [83] went further by introducing "active" thermal management concepts inside modified C/CCs

(C/C–SiC–ZrC–Cu) composites presented as combining passive ceramic protection with Cu-enabled heat dissipation during ablation, explicitly targeting reduced surface thermal response temperature rather than treating conductivity as a passive byproduct.

2.1.3. Gradient Architectures in Modified C/CCs and Manufacturability

A practical way to manage thermal conductivity (and the thermal stresses created by sharp property jumps) is to adopt gradient architectures, either as graded bulk modifications (e.g., graded UHTC infiltration) or graded coating stacks (transition layers and functional outer layers). Importantly, several studies show that gradients are not just conceptual, but they are manufactured using scalable, C/C-compatible routes.

On the bulk side, Wang et al. [84] reported gradient structured C/C-ZrC-SiC composites fabricated via reactive melt infiltration plus Chemical Vapor Infiltration (CVI), and they attributed the improved ablation performance to a synergy between a dense oxide layer and heat transfer through a retained pyrolytic-carbon network within the gradient structure, i.e., the gradient was used to satisfy competing needs (ablation resistance, mechanical integrity, and lightweighting) rather than optimizing a single metric [84]. On the coating side, gradient and transition-layer designs are repeatedly justified to mitigate thermal mismatch and cracking. Here, a $ZrSi_2$-SiC/SiC gradient coating study explicitly frames the gradient architecture as a solution to coating densification and thermal-mismatch limitations, implemented using a SiC transition layer and supersonic air plasma spraying of the outer layer [85].

From a manufacturing standpoint, the feasibility of gradient architectures depends strongly on where the gradient is located and how it is produced. Near-surface gradients and multilayer/graded coatings are the most immediately manufacturable because they can be created by staged deposition or staged conversion while keeping the interior architecture unchanged; this reduces risk because only the near-surface region is compositionally complex, and the carbon composite core remains process-familiar [86,87]. Volumetric gradients—where the matrix composition and porosity vary through thickness—are also feasible (as the recent RMI gradient UHTCMC studies show), but they are more sensitive to scale-up because infiltration depth, local capillarity, reaction kinetics, and thermal gradients can change across large parts, making gradient reproducibility and defect control (closed porosity, unreacted phases, local brittle zones) more challenging [65,88]. Therefore, for modified C/CCs, gradient architectures are technically well-motivated and increasingly validated for modified C/CCs in EE-like ablation conditions, but the most "selection-ready" pathways are those that confine complexity to engineered transition layers and near-surface gradients (where stress and oxygen ingress are managed) while preserving an interior carbon-rich architecture for compliance and damage tolerance. The limiting manufacturing issues are not conceptual, but are repeatability, inspection/qualification of gradient quality, and durability under cyclic thermo-chemical loading, which should be stated explicitly as the next barriers to broad deployment [65,87,89].

2.1.4. Ablation/Oxidation Behavior of Modified C/CCs (UHTCMCs)

Modifying components in this context refers to the as-discussed HECs (HECCs, HENs, HEBs, HEOs), which are monolithic refractory ceramics of certain transition metals and commonly include SiC ceramics. Notably, researchers are also exploring various strategies to enhance the oxidation and mechanical properties of C/CC with more complex reinforcements (e.g., SiCWs) for aerospace applications operating in exceptionally high temperatures [90–92]. These components can create glassy phases upon oxidation. Within the group of UHTCs, the refractory carbides HfC, ZrC, TaC, and SiC appear to have some of the highest melting points. These temperatures are similar to or surpass the sublimation

temperature of C/CCs, as well as the flame temperatures of most fuel-oxidizer combinations [93]. Since HECs have been studied to show better performance than monolithic ceramics, they can also be classified as good candidates for modifying C/CCs necessary for EEs. A comparative overview of these oxidation protection strategies is presented in Table 3.

Table 3. Comparison of oxidation protection strategies for C/C composites in extreme environments.

Strategy	Temperature Capability (°C)	Oxidation Protection	Thickness Impact	Durability	Key Advantage	Key Limitation	References
SiC Coatings	~1400–1700	Moderate	Low–Moderate	Moderate	Self-healing oxide layer	Glass-phase softening	[11,94,95]
UHTC Coatings (ZrB_2, HfC)	>2000	High	Moderate	Moderate	High temperature stability	Cracking/spallation	[4,71,96,97]
HEC Coatings	~1800–2200	Promising	Moderate	Low–Moderate	Tailorable chemistry	Limited long-term data	[72,94,98]
Multilayer/Gradient Coatings	>2000	High	Moderate–High	High	Reduced thermal mismatch	Processing complexity	[70,85–87,89]
Bulk Modification (UHTCMC)	>2000	High	High	High	Integrated protection	Increased density	[6,65,73]

Table 3 shows a clear progression in oxidation protection capabilities with increasing system complexity and cost. SiC represents the simplest approach, appropriate when surface temperatures remain below ~1700 °C where self-healing via silica formation is effective. Beyond this range, glass-phase softening and volatilization limit their reliability. UHTC coatings extend protection beyond 2000 °C, but their susceptibility to cracking and spallation under thermal cycling restrict their use as single-layer systems. Multilayer or gradient coatings address this limitation by reducing thermal mismatch, making them the most suitable option for reusable structures exposed to repeated aerothermal loading, albeit with higher processing complexity. HEC coatings offer tunable compositions but currently lack sufficient durability data, limiting their use to exploratory applications. Bulk modification (UHTCMCs) provides the highest combined temperature capability, oxidation resistance, and durability, but at increased density and cost, and is therefore reserved for cases where coating-based solutions are insufficient. The data from Table 3 supports a layered selection strategy: begin with SiC coatings where temperatures permit, transition to UHTC or gradient multilayer coatings for higher-demand reusable applications and adopt bulk UHTCMC modification only where coatings alone cannot provide the required protection.

Notable researchers such as Tang et al. [97] investigated the ablation characteristics of a ZrB_2-SiC coated C/CC, produced using high-solid-loading slurry impregnation (HSLSI) followed by Polymer Infiltration and Pyrolysis (PIP). The ZrB_2 slurry layer was maintained on the substrate and subsequently densified with the substrate during the PIP process to create the ZrB_2-SiC-integrated C/CCs. The ablation performance of this composite demonstrated significant reductions in mass ablation and in linear ablation rates after exposure to the flame for 60 s, 120 s, and 300 s, respectively. Typically, the inner layer, composed of ZrB_2-SiC, functioned as a barrier against oxygen, heat, and flow, thereby slowing down the oxidation rate of the substrate. This also indicates a robust adhesion between the coatings and the substrates. Xu et al. [99] explored the combined oxidation and mechanical properties of C/C-ZrC-SiC composites following laser ablation using a hybrid method of isothermal CVI and RMI in air. The reinforcement for these composites consisted

of a 2.5D needle-punched high-textured PyCF preform. In summary, the C/C-ZrC-SiC composites demonstrated excellent resistance to ablation and preserved bending strength, attributed to the oxidation of ZrC- SiC, evaporation of SiO_2, migration of liquid ZrO_2-SiO_2, and the infiltrated and grown ZrO_2. However, the ablation damage caused a transition from pseudo-plastic to brittle rupture, which may be attributed to the combined effects of rapid cooling, thermal stress, microstructure, and oxidation, which degrades the material's ability to undergo plastic deformation.

Silicon carbide whiskers (SiCWs) have also been used as a toughening mechanism for C/CCs. Figure 5 summarizes the typical preparation processes and reinforcement mechanisms of these SiCWs-reinforced composites. This improved toughness is due to the SiCWs' ability to bridge cracks and undergo pullout and growth, mainly when the crack spreads perpendicular to the whiskers' length. As preparation techniques advance, several similar studies [100–108] have been conducted on various kinds of SiCWs-reinforced multiphase and multilayer coatings to enhance the oxidation resistance of C/CCs. To address the issue of sealing a loose structure using traditional HfC, ZrC, and HfC-ZrC coatings on C/CCs against SiCWs, Li et al. [96] used a different reinforcing component (TiO) to tackle this. A HfC-ZrC-TiC multiphase coating was developed through supersonic atmospheric plasma spraying, then evaluated under Ees, such as a heat flux of 2.38 MW/m^2 and temperatures exceeding 2100 °C. Experimental findings showed significant improvements as the mass ablation rate dropped from 0.85 mg/s to 0.18 mg/s, and the linear ablation rate decreased from 2.58 μm/s to 0.71 μm/s within a period of 30 to 120 s. The mechanism behind this phenomenon reveals the self-healing properties of the HfC-ZrC-TiC coating and its enhanced ability to resist ablation at temperatures above 2100 °C, due to the active diffusion of TiO.

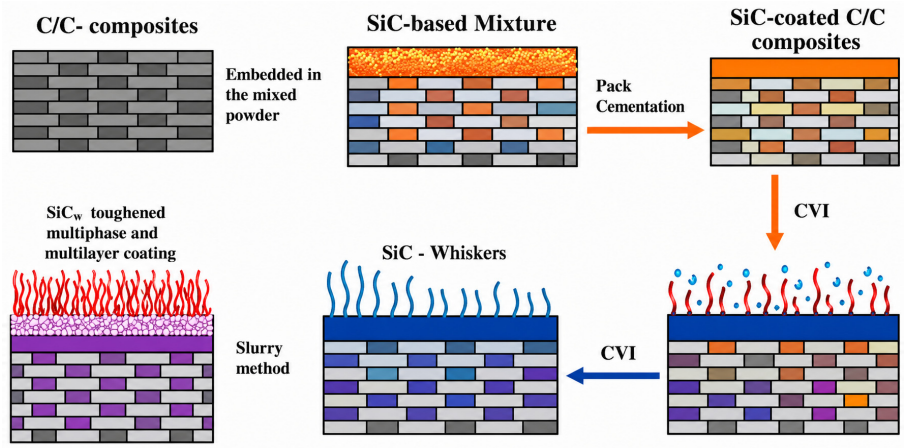

Figure 5. Diagram of the standard process for creating silicon carbide whisker SiCW-reinforced multiphase and multilayer coatings [109].

This performance was notably better than that of the commonly used SiC coatings and their whiskers, which tend to form glassy phases at temperatures between 1100 °C and 1650 °C during ablation [94]. While more notable properties such as ablation time, temperature and rate, and heat flux and strength have been reported on these composites, only a few studies have been conducted on the fracture toughness of these composites at extreme elevated temperatures, as evident in Table 4. It is therefore imperative to conduct detailed experimental and computational studies on the fracture toughness of these composites with consideration for the applications of accurate and cost-effective physics-based modeling, simulation tools, and cost-effective manufacturing processes.

Table 4. Key mechanical and thermal properties of UHTC-modified C/CC systems (C/C–UHTCs) and related UHTCMCs.

Materials	Methods	Ablation Method	Ablation (Mass/Linear) Time (s)	Ablation (Mass/Linear) Rate ($mgs^1/\mu m/s$)	Strength (MPa)	Fracture Toughness ($Mpa.m^{1/2}$)	Heat Flux (MWm^{-2})	References
Cf/HfB_2-C matrix	CVI	OAT	20 60 300	0.71 1.33 3.17	- - -	- - -	17 17 17	[50]
		OPT	20 60 300	0.81 2.82 7.84	- - -	- - -	4.4 4.4 4.4	[50]
Cf/ZrB_2–SiC	(HCVI)	AHWTT	650	-	148	5.6	-	[110]
2D Cf/ZrB_2–SiC	CVI + SI	OAT	20	8	237	-	4.2	[111]
3D-Cf/C–SiC–ZrC	RMI	OAT	60	1.21	143.5	-	4.18	[109]
3D-Cf/SiC–ZrC–TiC	RMI	OAT	60	0.008	-	-	-	[112]
Cf/(Hf1/2Zr1/3Ti1/6)C	PIP + SI	OAT	-	-	219.34	-	4	[113]
2D-Cf/C–HfB_2	PIP + CVI	OAT	90	2.75			4.18	[31]
C/C-Zr-SiC	PIP	OAT	120	-	-	-	-	[113]
C–C/ZrB_2 C–C/ZrB_2– SiC C–C/ZrB_2–$SiCLaB_6$ C–C/HfB_2 C–C/HfC	CVI + SI	OAT	60 30	0.67 0.63 0.74 0.57 1.69 0.22 0.18 0.17 0.77 0.55	-	-	2.38	[114]
C/SiC-HfC (H1) C/SiC-HfC (H2) C/SiC-HfC (H3) C/SiC-HfC (H4)	RMI	PWT	600 600 60 60	H2 > H1	-	-	3.5 3.5 4.4 5.0	[115]
Cf/HfC-SiC	SI + PIP	OAT		0.33	328.9	10.2 ± 1.2		
2.5D C/C-HfC-ZrC	PIP + RMI	OAT	600	0.544			4.18	[116]
Cf/ZrB_2-SiC-Y_2O_3 Cf/ZrB_2-$MoSi_2$ Cf/SiC-$Y2O_3$	HEBM + SI + SPS	BULF	60 60 60	−7.05 −0.56 −4.51	-	-	-	[117]
Cf/ZrB_2	SI + SPS	AJT	120	-	-	-	-	[118]
(PyC-Csf)/ZrB_2-SiC-ZrC	RSPS	OAT	120	3.41	-	-	2.38	[119]
Cf/ZrB_2-ZrC-SiC	PIP + RMI	OAT	120	6.67	-	-	-	[120]
Cf/ZrB_2-SiC-Y_2O_3	SI + PIP	APF	3000	0.33 μm/s	354.1	-	2.7 m^3 h^{-1}	[121]
3D-Cf/HfC–SiC	PIP	PWT	600	0.87	-	-	-	[122]
SiC nanowire network-modified C/C-ZrB_2-ZrC-SiC	PIP	Plasma torch	30	0.11 $mg{\cdot}cm^{-2}{\cdot}s^{-1}$/ 0.08 μm/s	-	-	-	[123]
2.5D C/HfC-SiC (SiC/HfC ratio study)	Isothermal CVI + PIP	OAT	60	0.29 ± 0.02 $mg{\cdot}cm^{-2}{\cdot}s^{-1}$/ 0.003 ± 0.0002 mm/s	203.4 ± 26.8	10.0 ± 0.5	-	[124]
C/C-HfC-SiC	RMI + GSI	Plasma torch	240	0.12/−0.22 μm/s	-	-	4.9	[125]
Functionally graded C/C-HfC-SiC	PIP + CVI	OAT	120	3.10 ± 0.26 μm/s (linear recession)	-	-	4.2	[126]
C/C–HfC–SiC	RMI (Hf–Si alloy)	OAT	300	8.9×10^{-3} mm/s	237 (flexural)	-	-	[127]

Note: Abbreviations for various method used as highlighted in Table 4: Air Plasma Flame (APF), Oxyacetylene Torch (OAT), Oxypropane Torch (OPT), Heaterless CVI (HCVI), Arc-Heated Wind Tunnel Test (AHWTT), Vacuum-Bag Infiltration (VBI), Arc-Jet Test (AJT), Plasma Wind Tunnel (PWT), Bottom-Up Loading Furnace (BULF), Solid–Liquid Combination (SLC), Supersonic Atmospheric Plasma Spraying (SAPS), gaseous Si infiltration (GSI), Reactive Spark Plasma Sintering (RSPS), Hot Isostatic Pressing (HIP), High Energy Ball Milling (HEBM).

Despite the heterogeneity of the reported datasets, Table 4 supports three analytical conclusions. First, among systems tested under comparable oxyacetylene or arc-jet conditions, lower ablation rates are generally associated with denser microstructures and more effective infiltration/densification routes, indicating that transport porosity control is a primary determinant of survivability. Second, residual strength, where reported, tends to remain higher in architectures with better microstructural closure and oxidation-resistant multiphase matrices, suggesting that durability depends not only on chemistry but also on crack-path management and pore connectivity. Third, the table reveals a major literature gap: fracture toughness and post-ablation damage tolerance are rarely reported, preventing rigorous ranking of reusability or structural reliability across modified C/CC systems. Thus, Table 4 is interpreted not only as a performance summary, but also as evidence that future materials selection should prioritize microstructure closure and stress-managed architectures before chemistry-only optimization.

2.1.5. Material Selection Rationale for Modified C/CCs

The preceding subsections have rightly established that no single modified C/CC system simultaneously optimizes mass efficiency, oxidation resistance, fracture toughness, thermal management, and manufacturability. Material selection is therefore inherently a trade-off governed by mission-specific requirements. To translate the preceding analysis into practical guidance, a structured material selection framework is presented in Table 5.

Table 5. Decision framework for material selection in extreme TPS.

Mission/Environment Condition	Recommended Material System Selection	Engineering Rationale
Peak surface temp $\leq$ 1400 °C; single-use acceptable	PICA or equivalent ablative TPS	Mass-efficient solution with extensive flight heritage; ablation eliminates need for oxidation resistance or thermal cycling durability
Peak surface temp $\leq$ 1700 °C; reusable; moderate load	C/C–SiC (RCC-type) with SiC coating	Protective SiO_2 layer provides oxidation resistance; proven reusable performance below SiC volatilization threshold
Peak surface temp 1700–2000 °C; reusable; moderate load	UHTC multilayer/gradient coating on C/C (e.g., ZrB_2–SiC, HfC-based)	Gradient architectures reduce thermal expansion mismatch; UHTCs enhance oxidation resistance at elevated temperatures
Peak surface temp 1700–2000 °C; reusable; high load (e.g., sharp leading edges)	UHTCMCs (Cf/ZrB_2–HfC via RMI or PIP + CVI)	Integrated structure and protection; improved fracture toughness enables load-bearing under extreme thermal flux
Peak surface temp > 2000 °C; reusable (emerging systems)	HEC-modified C/C or C/C–HECCs	Entropy-stabilized phases delay oxide scale degradation; promising for ultra-high-temperature regimes but limited validation
Oxidation-free environment (vacuum, inert atmosphere) up to ~2000 °C	Baseline C/C (unmodified)	Mass-optimal with highest toughness-to-density ratio; coatings unnecessary in absence of oxidation
Any temperature where coating breach and thermal cycling are dominant risks	Gradient/multilayer coating architecture (avoid single-layer UHTC)	Gradient layers relieve thermal mismatch stresses and maintain protection despite crack formation
Manufacturing scalability and cost are primary constraints.	C/C-SiC (CVI or PIP) or UHTC-coated C/C (plasma spray)	CVI/PIP routes are mature; plasma-sprayed UHTC coatings offer scalable protection; UHTCMCs provide performance but at higher cost and complexity

Table 5 provides a practical screening tool for initial material selection. The framework reflects the core finding of this review: material selection for extreme aerospace environments is not a single-parameter decision but a coupled trade-off between temperature capability, reusability, structural demand, and manufacturing feasibility. Final design decisions should incorporate additional considerations including component geometry, thermal gradient profiles, manufacturing route constraints, and available validation data for the specific operating environment.

3. Manufacturing of C/CCs

The manufacturing of C/CCs and their modified variants involves several densification and infiltration techniques, each with distinct advantages and limitations in terms of processing time, scalability, cost, and defect sensitivity [6,128]. The most widely used methods include CVI, PIP, and RMI, among others, each discussed in detail in the following sections. A comparative assessment of these manufacturing routes is summarized in Table 6. Regardless of the densification route selected, all modified C/CC manufacturing pathways share a common starting point: the design and fabrication of the carbon fiber preform, which governs permeability, anisotropy, and damage tolerance throughout all subsequent processing stages [5,129].

Table 6. Comparative assessment of manufacturing methods for C/C and modified composites in terms of scalability, cost, and defect sensitivity.

Method	Processing Time	Scalability	Cost Level	Defect Sensitivity	Key Advantage	Key Limitation	References
CVI	Very high (100–1000 h)	Low–Moderate	High	Low porosity but slow densification	High-quality matrix	Long processing time	[6,130]
PIP	Moderate–High	Moderate	Moderate	High shrinkage/porosity	Flexible chemistry	Multiple cycles required	[6,128]
RMI	Low–Moderate	High	Moderate	Risk of cracking/thermal stress	Fast densification	Reaction control complexity	[65,73]
Slurry Infiltration (SI)	Moderate	Moderate	Low–Moderate	Particle filtration issues	Simple processing	Limited penetration	[77,97,128]
RF-CVI/Advanced CVI	Low–Moderate	Emerging	Moderate–High	Process complexity	Reduced cycle time	Equipment complexity	[131,132]
Simplified Infiltration-Free (SIF)	Low	Emerging	Low	Limited validation	Reduced processing steps	Early-stage technology	[133]

3.1. Build the Fiber Preform

C/CCs begin with a CF architecture chosen for the load path and through-thickness needs: stacked 2D cloth, needled "2.5D," or fully 3D braided/orthogonal weaves. These preforms set permeability (how a matrix precursor flows), pore size/connectivity, and anisotropy. A recent work by Tan et al. [134] detailed the comparison of 2.5D needled vs. 3D braided preforms as shown in Figure 6 and their pore structures, then densified them by isothermal chemical-vapor infiltration (ICVI) at ~1100 °C using natural gas. Agarwal et al. [5]'s review also summarized modern C/CCs architecture and processing routes.

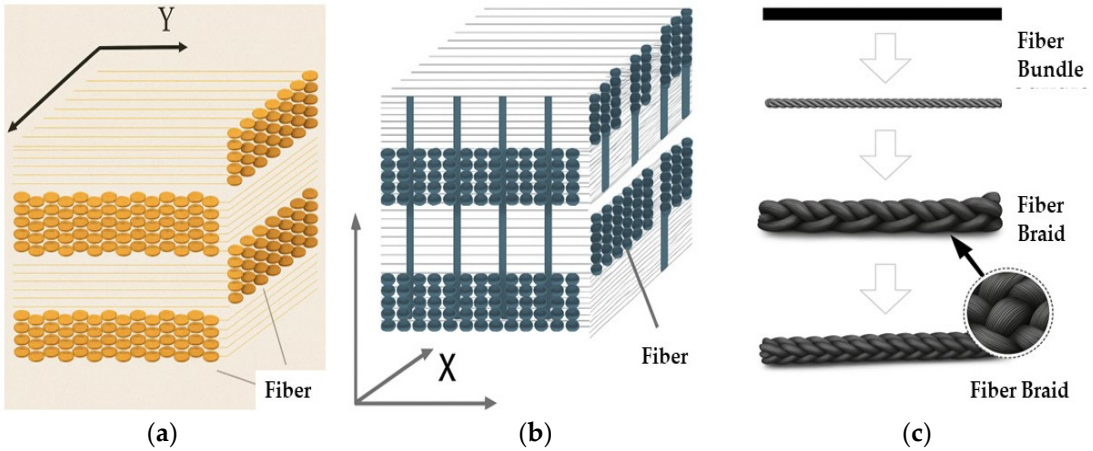

Figure 6. Architecture of preform for C/C composites, (**a**) 2D C/C composites; (**b**) 2.5D C/C composites; and (**c**) 3D C/C composites, respectively [133].

3.2. Resin Impregnation and Densifying the Carbon Matrix (Two Mainstream Routes)

The first mainstream route of impregnating and densifying the carbon matrix is commonly known as Liquid/Polymer Infiltration and Pyrolysis (PIP or "LPI"). The major advantages and disadvantages of these manufacturing processes have been outlined in Table 7. These Carbon Fiber Reinforced Composite (CFRC) production methods could also be applied for a controlled densification of C/CCs using a low-temperature polymeric precursor. However, these processes do not provide completely adequate solutions for the manufacture of C/CCs suitable for EEs because a higher temperature is usually needed for obtaining porous structures that allow for further densification and improved properties. Current advancements in CFRC production aim to align CFs' benefits with the simpler manufacturing of metallic parts [135]. In this regard, the carbon phenolic–prepreg route allows for the rapid fabrication of complex shapes needed for initial carbonization, and then re-impregnation with resin or resins embedded with ultra-refractory phases directly into the carbon matrix. This yields a composite that still char-protects like classic C/CCs but now has a ceramic-enhanced surface layer that resists oxidation and pining cracks. Because it adds complexity and cost, the method is usually suited to high-value components (sharp leading edges, nose cones, or re-entry vehicles) where weight and reusability are critical.

Table 7. Merits and demerits of key manufacturing methods for CFRCs [129].

Fabrication Methods	Merits	Demerits
Low Temperature Methods (Liquid Precursor Infiltration)		
RIDFT	Uses affordable resin materials and allows for simple management of 2D impregnation.	It can make only formable geometries.
SCRIMP	Maintain consistency across dimensions.	Preforms with high permeability are required.
RTM	Achieve similar quality levels using an autoclave.	Production is limited due to constrained space, leading to batch manufacturing.
Quickstep	Precise regulation of temperature.	Finite duration of a flexible membrane's presence.
VBO	Many components are made during each manufacturing phase.	Lesser heat transfer occurs compared to an autoclave.
VARTM	Simple management of 2D impregnation.	Restrictions of resin to reach the desired amount of fiber in a material.
Resin Film Infusion (RFI)	There is no necessity for repeated debulking operations.	Placing resin film into a mold requires a lot of work.

Note: Resin Infusion Between Double Flexible Tooling (RIDFT), Seemann Composites Resin Infusion Molding Process (SCRIMP), Resin Transfer Molding (RTM), Vacuum Bagging Operation (VBO), Resin Film Infusion (RFI).

3.3. High-Temperature Heat Treatment: Carbonization and Graphitization

In most cases, the typical second mainstream in manufacturing porous C/CCs is known as carbonization, where the CFRC created in the first stage is subjected to high temperatures (typically 800–1100 °C) in an inert atmosphere (like argon or nitrogen). This process tends to decompose the resin, leaving behind a carbon matrix around the CFs and removing any volatiles in the formation of a porous C/C preform. The carbonized composite, which typically still contains voids and pores, is then re-impregnated with a precursor (such as pitch or resin, ceramic slurry/modified resins) using various high-temperature techniques such as CVI, PIP, RMI, slurry infiltration (SI), hydrothermal reaction, in situ reaction, HIP, and sol–gel methods, and then re-carbonized [128,136–148]. Figure 7 schematically illustrates high-temperature methods of fabricating modified C/CCs. These manufacturing processes have been explained in detail in several research papers [128,139]. Hence, Table 8 highlights the key advantages and disadvantages of some of these methods.

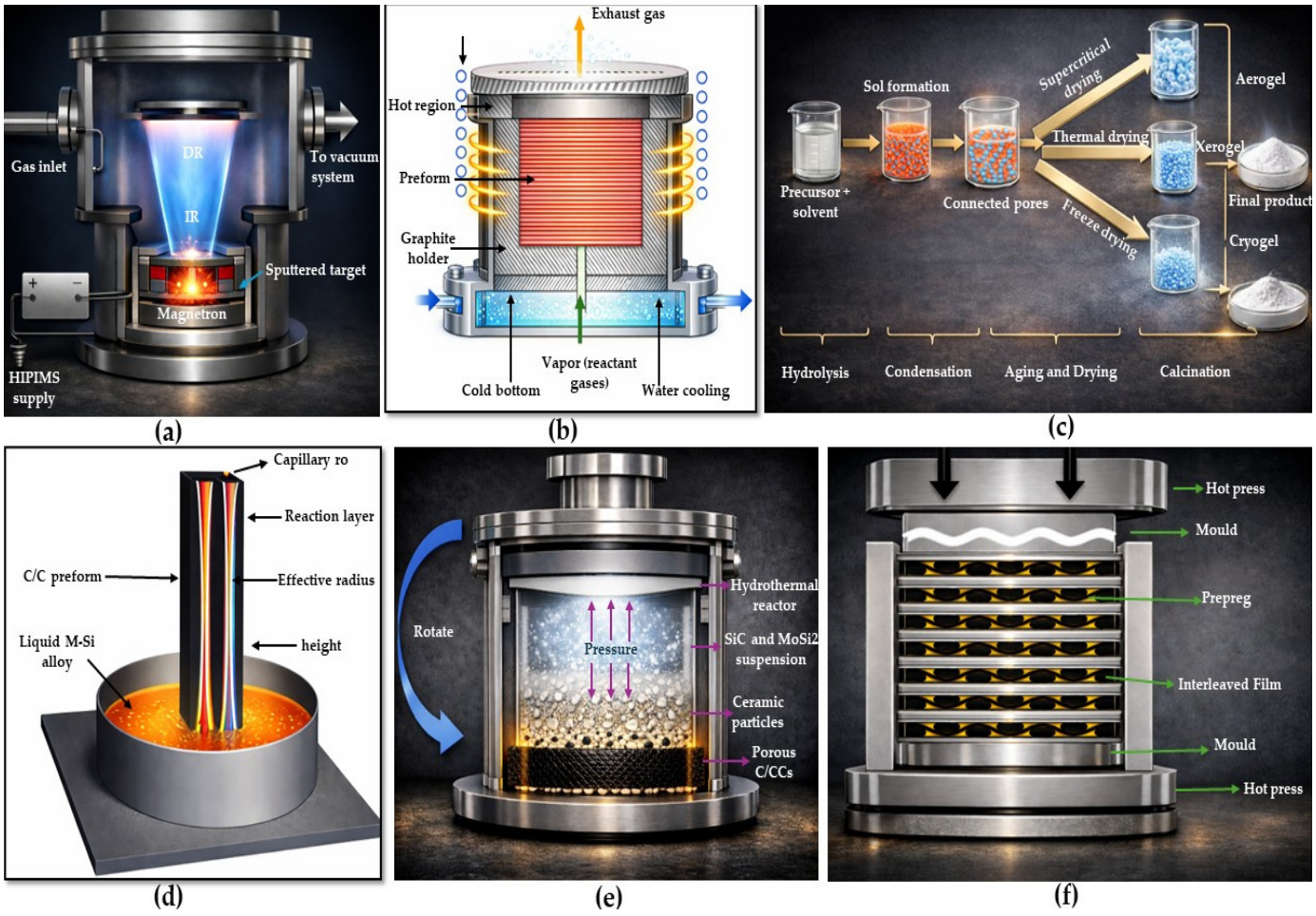

Figure 7. Common fabrication methods for second stage modification of C/CCs: (**a**) magnetron sputtering (MS) [140], (**b**) CVI [130], (**c**) sol–gel [141], (**d**) RMI [142], (**e**) hydrothermal reduction [143], and (**f**) hot pressing (HP) [144].

Table 8. Advantages and disadvantages of key manufacturing methods for modified C/CCs [6].

Methods	Advantages	Disadvantages
PIP	A ceramic deposit can have a wide range of compositions because of the varied chemistry of its precursor materials.	Low ceramic yields from the precursor necessitate multiple cycles of infiltration and pyrolysis to achieve the desired density. This process increases both the time and cost for producing a component.

Table 8. *Cont.*

Methods	Advantages	Disadvantages
RMI	The processing time is shorter compared to most ceramic matrix composite manufacturing methods, making it relatively inexpensive.	The reaction's exothermic nature can raise the temperature in the immediate area, leading to increased damage.
CVI	Impregnation processes are simple, needing just impregnation and drying, to moderately increase the density of the green composite.	Limited penetration into fiber bundles happens because the particles are too big compared to the size of the fiber bundle openings.
SI	Apparatus is the same used for sintering monolithic ceramics.	The equipment used is identical to that employed for sintering solid ceramics.
Pressure Sintering (PS)	Theoretically, lower pressure decreases the chances of interaction between the matrix and fibers as well as reduces the risk of fiber degradation.	For low pressures, higher sintering temperatures and longer times are needed compared to Hot Pressing (HP) and Spark Plasma Sintering (SPS).
HIP	The chemicals in question have relatively minor health and safety concerns, especially when compared to PIP and CVI.	The equipment used in this process is costlier than traditional HIP and pressureless furnaces.

3.4. Post-Processing, Finishing, and Joining

After densification/heat-treatment, C/CC parts are precision-finished, which involve trimming edges, milling profiles, and drilling holes under tightly controlled parameters (feeds/speeds, backing, and dust control). The NASA process specification for composites formalizes trimming/drilling practices; for delicate C/C geometries (e.g., grids), ultrasonic drilling is often preferred over conventional cutting due to fiber pull-out and edge damage risks [145,146]. Finishing also includes contamination control and safe handling (sharp-edge removal, debris management) to protect both hardware and personnel [147]. For joining, C/CCs structures can be mechanically attached (bolted interfaces, as on Shuttle RCC wing leading edge panel sets) or metallurgically joined to metals using active-metal brazes (e.g., Ti, Cusil-ABA), which promote wetting and interfacial reaction; the design must manage wetting behavior and CTE mismatch to avoid residual-stress damage [148,149]. The general fabrication processes of C/CCs are depicted in Figure 8.

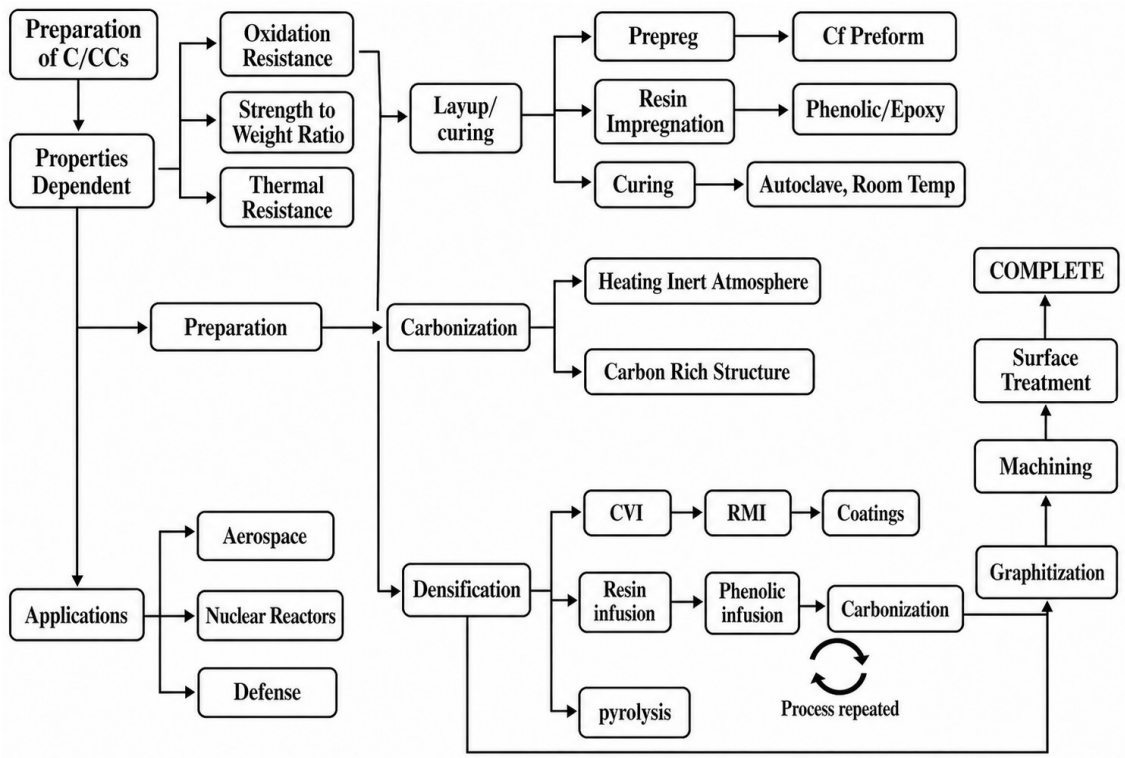

Figure 8. General preparation steps for C/CCs.

3.5. Oxidation Protection of Modified C/CCS via Thermal Spraying

Bare C/CCs oxidize quickly above ~450–500 °C in oxygen-containing environments, and so external environmental barrier coatings are standard. The initial stage in developing anti-oxidation strategies/coatings for C/CCs focuses on using refractory formulations with monolithic ceramics [17,150] due to their high melting points and oxidation-resisting capabilities [54,151–158]. These systems, when applied through thermal spray methods, could shield C/CCs from oxidation at significantly higher temperatures [159]. Thermal spraying provides scalable deposition routes for oxidation and ablation barriers on modified C/CCs. For carbon-based TPS, the process choice is governed by whether the deposited layer can achieve low connected porosity, robust adhesion, and a stable stress/crack state, because any connected defect network (pores or cracks) becomes an oxygen/oxidant pathway that undermines protection [95]. Table 9 briefly maps key thermal spraying methods relevant to the selection of modified C/CCs. Within the thermal-spray family, high-velocity methods such as HVOF and detonation gun tend to produce denser deposits with higher adhesion and lower porosity than conventional flame spray, while plasma-based routes are often necessary when depositing UHTC carbides/borides due to their ultra-high melting points. However, plasma spraying also elevates residual-stress and cracking risks due to rapid quenching and thermal gradients, which must be managed via process control and architecture (e.g., graded layers, compliant interlayers, sealing) to avoid through-thickness crack pathways. Cold spray is discussed primarily as a low-thermal-impact interlayer/repair strategy (rather than a direct UHTC topcoat route) because it is best suited to ductile materials and can introduce compressive stress states that can be advantageous for interfacial integrity.

Table 9. Thermal-spray routes: relevance to modified C/CC oxidation and ablation coatings (selection-oriented).

Thermal Spray Route	Coating Quality and Adhesion	Residual Stresses and Cracking Risk	Oxidation and Ablation Protection Relevance	Scalability/Suitability for Modified C/C	References
High velocity oxygen fuel	Dense, low-porosity coatings with strong adhesion	Lower thermal input than plasma spray	Direct role in UHTC topcoats is more limited than plasma routes.	High industrial maturity; scalable to large components	[159,160]
Flame spraying	Higher porosity and lower bond strength than HVOF	Crack/porosity connectivity is a key concern for carbon substrates	Higher connected porosity and lower adhesion increase risk	Very scalable and low cost, but typically not preferred for EE oxidation and ablation barriers on C/CC	[95,161,162]
Detonation gun	Very dense coatings, high adhesion strength, and low porosity	Generate beneficial compressive residual stresses	Attractive where a dense barrier is needed and where chemistry can be deposited without excessive decomposition	Best positioned for high-value localized protection	[163,164]
Cold spray	Can yield good adhesion with minimal heat-affected zone	Produces compressive residual stress states due to peening, with minimal thermal mismatch	Direct spraying of fully ceramic UHTC barriers is limited	Scalable and attractive but serve as an interlayer strategy, not as a stand-alone UHTC barrier route	[165–167]
Plasma spray	Most relevant when depositing very high-melting UHTCs	Residual stresses arise from quenching and thermal gradients	Widely used for UHTC barriers precisely because it can process UHTC compositions	High industrial maturity and scalability; often the most realistic route for UHTC topcoats on C/CC	[168,169]

3.6. Manufacturing Cost Impact

The two dominant obstacles to using C/CCs as structural TPS are (i) high, multi-cycle manufacturing cost, and (ii) oxidation vulnerability of carbon at high temperatures—hence, the widespread use of Si/SiC-family and UHTC/HEC-containing coatings whose effective temperature/pressure windows remain bounded. On the cost side, classical PIP/CVI routes demand many impregnation–pyrolysis cycles or long CVI times, plus high-temperature carbonization/graphitization, and specialized tooling/non-destructive evaluation (NDE), hence, driving labor and capital charges. NASA's heritage summaries and handbooks have long flagged C/CCs as time-consuming and expensive relative to metals or polymer composites. Contemporary CVI reviews and program notes reiterate that ICVI can require weeks (1000 h) to close porosity; in contrast, forced-flow/thermal-gradient CVI (FCVI/TG-FCVI) and related variants reduce densification to hours (<1 day) for thick sections by imposing pressure and thermal gradients, but at the expense of added fixturing/complexity [170].

Two newer, cost-focused approaches illustrate the state of the art (1) radio frequency (RF)-assisted CVI ("inside-out" thermal gradient)**:** Venkatachalam et al. [171] densified 2.5D carbon preforms pre-filled with ~30 vol% ZrB_2 via RF-CVI, producing Cf-UHTCMCs rapidly and demonstrating order-of-magnitude cycle-time reductions relative to conventional CVI; reports showed that standard CVI can "easily take ~1000 h," while RF-CVI enables near-net-shape pyrolytic carbon (PyC) fill at ~1000 °C and faster turnaround, with arc-jet-style thermal qualification above 2000 °C. This directly targets CVI time/labor cost in C/CC-derived UHTCMC parts. (2) SIF CMCs: Wei et al. [133] eliminated the infiltration step by using an 84% high-char-yield preceramic resin with functionalized SiC particles cured under vacuum/compression, then pyrolyzed in a controlled atmosphere, reporting a manufacturing cost of ~$300/kg versus $500/kg for a 2-cycle PIP CMC, i.e., a >50% cost reduction mainly from labor/time saved (fewer cycles). While their SIF route still needs a separate high-T pyrolysis to reach a C/C or C/SiC-type matrix (and thus cannot avoid the energy cost of carbonization), it shows how step count and handling dominate costs and where novel precursors can help.

Beyond those demonstrations, alternative acceleration routes continue to mature. Electromagnetic- or electric field-assisted CVI (E-CVI) has been used to fabricate thick C/CCs and C/SiC in "dozens of hours" rather than weeks, indicating that field-assisted mass transport can be a general lever on CVI cost [172]. RMI used for C/C-SiC remains attractive for near-net-shape, and fast fabrication with lower cycle count (trading CVI reactors for high-T melt handling and Si reactivity control). Parametric and review studies describe RMI as "fast and economical," provided porosity and capillarity are engineered for complete conversion without choking [173].

Therefore, the current cost levers for modified C/CCs (UHTCMCs) are to reduce time to densify, cut step count with high-char precursors or infiltration-free resin approaches where applicable, and to integrate processes to minimize re-fixturing and scrap. The floor on unit cost still reflects high-temperature energy demand, fiber and precursor prices, finishing, coating operations, and NDE. Still, the emerging demonstrations above show credible paths to faster throughput and lower labor content for TPS-relevant architectures.

It is worth noting that all modified C/CC concepts, including UHTCMCs- and HECs-based variants share the same manufacturing workflow, i.e., selection of carbon fiber precursor/architecture, fabrication of a 2D/3D preform, and subsequent densification (e.g., repeated liquid infiltration/pyrolysis) to build the carbon matrix and close porosity. In fact, aerospace heritage RCC systems were fabricated from woven carbon-fiber layups that were repeatedly infiltrated with carbon precursors, underscoring that fiber manufacturing and preform design are foundational steps that directly control anisotropy, damage tolerance,

and transport pathways in the final composite. However, the motivation to move from baseline C/CCs to ceramic-modified C/CCs is not merely incremental property tuning but fundamentally driven by environmental durability in oxygen-containing EE service.

4. Modeling/Tools Mapped to Selection and Certification

Materials for EEs face two coupled challenges: (i) intense thermal–mechanical loads dictated by geometry and placement, and (ii) reactive, oxidizing flows that drive property evolution (oxidation) and shape change (ablation). Modern NASA entry-systems works explicitly treat design as a material–structure–environment triad, advancing multiphysics ablation frameworks and micro-scale-to-macro-scale property upscaling so that screening windows (heat flux, strength, thermal conductivity, CTE, fracture/fatigue metrics, stagnation temperature) can be populated with higher-fidelity predictions.

NASA's micro-scale method for porous TPS is illustrative of modernizing macro-scale and maturing micro-scale ablation modeling tools, including shape-change coupling, and porous-TPS workflows [174–176]. Figure 9 illustrates the application areas of computational material modeling for composite structures.

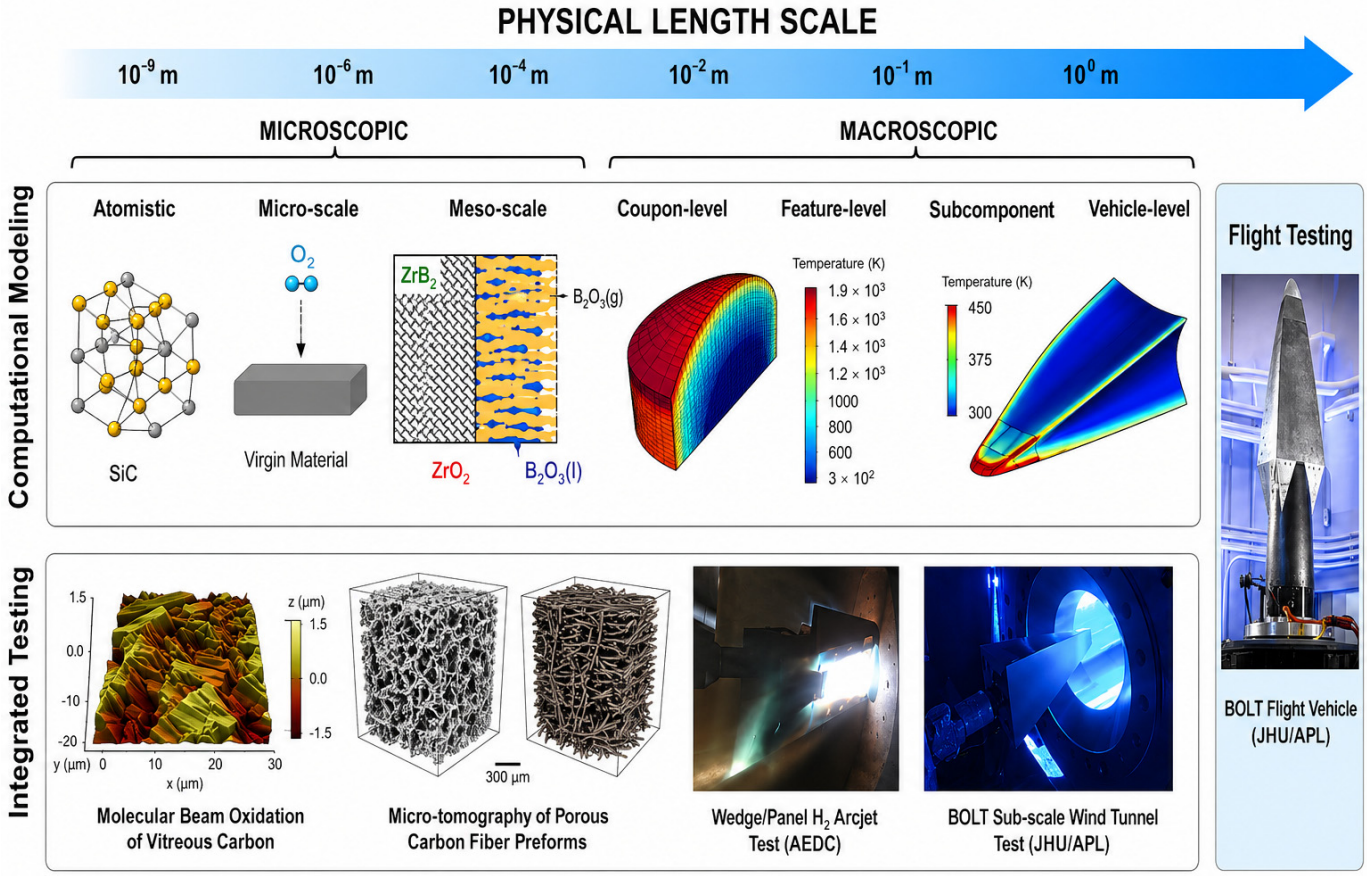

Figure 9. Domains of computational modeling software applications for materials design [3].

4.1. Nano-/Micro-/Meso-/Macro-Scale Material Modeling Tools

At the micro-scale, *image-based* modeling has become routine for fibrous carbons (e.g., FiberForm). NASA's Porous Microstructure Analysis (PuMA) extracts effective thermal, elastic, permeability, and anisotropy tensors directly from X-ray microtomography (XRCT), providing inputs to macro solvers; new releases add immersed-boundary solvers and broaden 3D/4D capabilities (tomography-to-properties) [131,132].

Recent Direct Simulation Monte Carlo (DSMC) advances in Stochastic Parallel Rarefied-gas Time-accurate Analyzer (SPARTA) add an active-site framework that reproduces etch-

pit nucleation and growth on carbon microstructures (e.g., FiberForm), thereby linking reactive gas–surface chemistry to microstructural evolution and the resulting drift in effective properties (quantified via PuMA) [133]. Together, these tools close the loop from microstructure to component response in ablation/oxidation environments.

At the macro-scale (component/system level), the upscaled micro/meso descriptors (effective thermal/elastic tensors, permeability, and evolving recession/pyrolysis kinetics) are embedded in multidimensional TPS thermal-response and thermo-structural simulations used for sizing and certification under mission-relevant entry environments. In NASA's TPS modeling toolchain, FIAT remains a widely used 1D thermal/ablation solver for sizing, while Two-dimensional Implicit Thermal response and Ablation (TITAN) and 3D FIAT address cases where multi-D conduction and internal gas flow become important; Icarus is being developed as a next-generation unstructured-mesh, HPC-oriented TPS solver intended to enable large, full-scale heatshield analyses and to be seamlessly coupled to modern hypersonic computational fluid dynamics (CFD) solvers for consistent boundary conditions (BCs) on complex geometries [22,177–179].

At the nanoscale, Density Functional Theory/Quantum Mechanics (DFT/QM) calculations remain the gold standard for chemistry, energetics, and interfacial reactions; practical exascale-oriented implementations (e.g., Quantum Espresso GPU ports) have lowered cost and widened problem sizes relevant to ceramic/graphitic interfaces [180]. To bridge the gap toward molecular dynamics (MD) while retaining ab initio accuracy, machine-learning interatomic potentials (MLIPs), notably equivariant graph neural-network models such as Neural Equivariant Interatomic Potentials (NequIP), deliver DFT fidelity at MD cost, enabling the simulation of chemically complex, high-temperature interface phenomena at relevant scales [181]. Interatomic Models (IMs) have also typically been integrated directly into MD simulation software, such as the Large-scale Atomic/Molecular Massively Parallel Simulator (LAMMPS), Quantum Espresso, Parallel Dislocation Simulator (ParaDIS), and Multiphysics Object-Oriented Simulation Environment (MOOSE). Nonetheless, this approach hampers reproducibility because both the simulation codes and IMs are constantly evolving [182]. Ensuring reproducibility/portability of IMs across codes has likewise progressed: the OpenKIM ecosystem and its KIM-based Learning-Integrated Fitting Framework (KLIFF) provide a standardized API, curated model repository, and learning-integrated workflows with uncertainty quantification, which are critical for cross-platform validation and auditability [183].

Crucially, the field is process-aware: models now propagate thermal history, pressure/dwell schedules, and porosity/void evolution from densification routes (CVI/PIP/MI) into structural property predictions and design envelopes. Recent studies demonstrate full-scale, multi-physics CVI modeling for large C/C parts ($\varnothing \approx 1.2$ m). At the same time, related work updates Isothermal CVI transport/kinetics for robust optimization. These resources could be well-suited to modified C/CCs screening workflow [184,185]. At the same time, ablation/oxidation reviews for C/Si-based composites synthesize mechanistic understanding at 1400–1700 °C, underscoring the need to couple gas–surface chemistry, internal transport, and microstructural evolution in design-ready tools [186].

In summary, state-of-the-art nano-/micro-/meso-scale composites design for EEs integrates: (1) ab initio accuracy where chemistry dominates; (2) MLIPs on standardized, auditable infrastructures (OpenKIM/KLIFF) for scalable MD; (3) image-based micro-scale ablation/oxidation modeling with property upscaling (PuMA + SPARTA); and (4) advanced continuum damage mechanics (phase-field/cohesive, high-performance computing (HPC) implementations) at component scale. Table 10 summarizes the significant applications of these models to C/CCs as well as their advantages and disadvantages.

Table 10. Modeling approaches and tools for C/CCs and TPS in EEs.

Category	Model/Tool	Major Application to C/CC & TPS	Advantages	Disadvantages	References
Nano-/Micro-scale	Quantum Espresso	Atomistic energetics/reaction pathways for C/CCs interfaces and UHTC/HEC oxidation chemistry	Active GPU/exascale development broadens problem sizes.	High cost & limited time/length scales	[180]
	NequIP with OpenKIM/KLIFF workflow	Near-DFT fidelity molecular dynamics of high-T interfaces, crack-tip chemistry, mixed phases	Model archiving/portability via KIM-API/KLIFF	Quality hinges on high-T training sets	[181]
	SPARTA with active-site/etch-pit capability)	Captures etch-pit formation in carbon (e.g., FiberForm), linking gas–surface chemistry to pore-scale morphology	Bridges to effective properties/ permeability for C/CCs.	Chemistry/kinetics for non-carbon ceramics above ~2000 °C are sparse	[187]
Meso-scale	Image-based upscaling (PuMA)	From XRCT of fibrous/woven C/CCs to permeability, anisotropy for input to macro material response solvers	Open source: meshes & solvers tailored to porous TPS; active development.	Requires accurate T-dependent constituent data; does not by itself model high-T oxidation/ volatility of UHTC/HEC scales	[188]
Macro (material response)	Icarus (US3D)	Multi-D ablators & hot structures: in-depth heat transfer & ablation	Parallel unstructured capability	Sensitivity to property/chemistry libraries	[178]
	CHAR	Multi-D heat conduction & charring with an FE core	Established FE framework for TPS; thermoelastic stress capability	Modernization & property libraries may lag for next-gen materials	[189]
CFD (aero loads)	RANS (VULCAN)	Rapid generation of aerothermal load envelopes as BCs for finite element analysis (FEA)	Predicts heat-flux peaks on C/CCs TPS	Often mispredict heat-flux peak	[190]
	LES/WMLES	Scale-resolving prediction of unsteady that drives heat-flux/pressure peaks on C/CCs TPS	Captures low-frequency dynamics & bubble size/location.	Higher computational cost	[191]
	DNS	Reference for hypersonic transition to calibrate WMLES/RANS used in TPS design	Available mechanism-resolving datasets at Mach ~5	Limited parametric/chemistry coverage for end-to-end design loop	[192]

Note: Abbreviations for various method used as highlighted in Table 10: Reynolds-Averaged Navier–Stokes (RANS), Viscous Upwind Algorithm for Complex flow Analysis (VULCAN), Large Eddy Simulation (LES), CHarring Ablator Response (CHAR).

This layered modeling/toolchain could enable credible, cost-aware screening and down-selection of RCC, UHTCMCs, UHTCs, HECs, and HEC-modified C/CCs under coupled thermal–mechanical–chemical loads. However, full, validated, cyclic-use prediction for UHTC/HEC-based reusable TPS above 2000 °C remains an unsolved problem. The limiting factors are high-T chemistry/phase data, micro/macro coupling under cycles, and scarce validation datasets. On a larger scale, continuum constitutive models using FEA-based computational modeling tools are effective at forecasting key properties like deformation response and thermomechanical behavior [193]. This analysis can be expanded to examine the contraction caused by polymerization or crystallization, the impact of fiber wrinkling, and the temperature variations that occur due to varying coefficients of thermal expansion between different materials. Nevertheless, accurately predicting damage progression, including fracture toughness, remains a challenging task for these models [22,177–179]. A more detailed overview of common computational modeling techniques, such as CFD and FEA, with their respective applications in composite structures design, are further discussed.

4.2. CFD

CFD is included here strictly as a materials-relevant tool for defining and iteratively updating the aerothermal BC that governs oxidation and ablation and in-depth thermal response. In modern entry toolchains, CFD supplies surface pressure, heat-transfer coefficients/recovery enthalpy, shear, and radiative environments that are consumed by material response solvers (e.g., PuMA/PATO/CHAR/Icarus) to predict temperature, pyrolysis/blowing, oxidation, and recession. Conversely, material response modifies the flow BC via surface temperature, roughness/recession, and pyrolysis blowing, motivating iterative CFD–material coupling; NASA demonstrations integrate PATO blowing products into Data-Parallel Line Relaxation (DPLR) via a blowing BC and iterate with radiative heating to obtain consistent heating/temperature histories for TPS down-selection. Additionally, carbon-based TPS requires wall models that account for catalytic recombination and ablation effects, which can significantly alter predicted heat-flux footprints relative to inert-wall assumptions [194–196]. Some CFD roles to deliver the surface environment and to model the wall physics that directly control C/CCs oxidation and ablation and response are briefly discussed.

4.2.1. Coupled CFD–Material Response Workflows for Ablation/Oxidation and Shape Change

In these workflows, CFD provides the time-dependent surface environment, i.e., convective heating, pressure, species, and (when available) radiative contributions, while the material response solver advances the in-depth thermal field, pyrolysis/blowing (if applicable), oxidation and ablation, and recession; the resulting surface temperature, mass addition (blowing), and surface state are then fed back to CFD to update the BC and close the loop. This coupling is particularly important for carbon-based TPS because surface recession and gas–surface chemistry can shift the local heating history in ways that a one-way (decoupled) approach cannot reliably capture when the interface conditions evolve rapidly [176]. NASA Ames' recent coupled demonstrations provide a clear template for how this is implemented in practice. In the PATO-DPLR–Non-Equilibrium Air Radiation (NEQAIR) loop, PATO computes the internal response and produces pyrolysis/blowing products; these gases are imposed in DPLR using blowing BCs, DPLR updates the aerothermal environment, and NEQAIR supplies radiative heating, with iterations continuing until surface temperature and heating histories are consistent [196].

4.2.2. Verification, Validation, and Uncertainty Quantification of CFD-Derived Loads for C/C TPS Life Prediction

NASA Langley's aerothermodynamic testing program continues to generate global heating datasets (including phosphor thermography), explicitly noting their use for CFD validation and for advancing mapping/reduction tools that convert measurements into surface heat-transfer distributions suitable for comparison with simulations [197]. Recent efforts also highlight improved diagnostic capability, e.g., quantitative infrared thermography campaigns designed for validation-grade heat-transfer data in hypersonic facilities, supporting a more robust experimental basis for bounding CFD wall heat-flux predictions that are subsequently used as TPS BCs [198]. Recent NASA overviews treat modeling and uncertainty as first-order requirements because inferring heat flux stagnation, pressure, and shear (and relating them to flight-relevant heat loads) govern how confidently arc-jet results can calibrate TPS material response models [199].

Therefore, the uncertainty quantification literature for hypersonic aerothermal predictions increasingly quantifies how parameter/model uncertainties propagate into wall heating, and hence, providing a defensible basis for using load bands (rather than single traces) when predicting recession, temperature margins, and life for carbon-based TPS.

4.3. FEA

FEA is included here not as a generic strength simulation, but as a durability and life-prediction framework that links mission aerothermal loads to thermomechanical damage accumulation and environmental degradation (oxidation and ablation, recession, and property drift) in C/CCs used in EE service. This focus is consistent with current hypersonic/TPS priorities, where reusability and reliability under aggressive oxidizing heat-flux environments are central sustainability metrics.

At the component level, FEA for EE-TPS typically couples (i) material response/thermal solvers that predict in-depth temperature, pyrolysis/outgassing, and recession with (ii) thermo-structural FEA that maps the evolving thermal field and geometry into stresses, distortion, joint loads, buckling margins, and damage indices. Figure 10 depicts the common FEA steps to obtain approximate values for the field variables, that are then interpreted and visualized, allowing engineers to analyze the behavior of the structure under the given conditions and then make informed decisions based on the FEA output. In NASA's predictive material-modeling ecosystem, this is reflected by tool chains where porous/material response models (e.g., PATO; validated against FIAT) are used alongside multi-D TPS solvers that scale to full-system analyses. Importantly, FIAT-class tools are described as extensively validated using arc-jet and flight data, underscoring that "useful" structural simulations must be anchored in validated material responses [3].

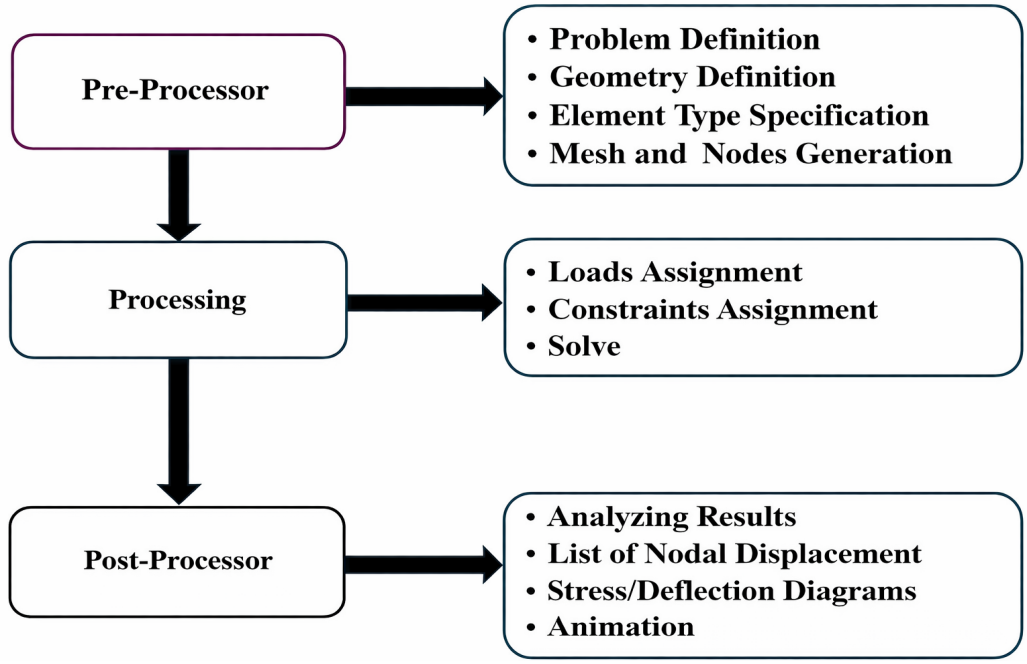

Figure 10. Overview of FEA computer simulation setup [200].

Critically, this coupled view is directly tied to C/CC sustainability in EE service because carbon's structural reliability is often limited by oxidation- and ablation-driven thickness loss and stiffness degradation, not by room-temperature strength. Recent thermo-chemo-mechanical modeling directions explicitly aim to couple oxidation and ablation (and internal transport/chemistry) with evolving stress states and damage, enabling life-aware design rather than one-off strength checks [201]. EE-relevant FEA scenarios are further discussed. These scenarios are explicitly tied to EE loads and to sustainability in the TPS sense (reusability margins, reduced refurbishment risk, fewer test iterations, less oversizing, and more reliable certification).

4.3.1. Thermal–Oxidative Thermal-Shock

Thermal shock in air is a coupled EE-style threat because oxidation and rapid heating jointly degrade load-bearing capability and can increase refurbishment burden. In a controlled thermal-shock study of 2D C/C exposed to 400–1000 °C in an oxidizing environment, compressive stiffness/strength decreased with increasing shock temperature, and microscopy distinguished different oxidation morphologies (e.g., more uniform internal attack at lower temperature versus more surface-dominated attack at moderate temperature), motivating protective strategies to preserve structural integrity during high-T service [202]. A follow-on computational framework is positioned specifically to predict such thermo-oxidative property loss and thereby support design decisions (architecture/coatings/safety factors) aimed at extending service life rather than simply reporting strength.

4.3.2. Architecture-Resolved Multiscale Finite Element (FE) for Anisotropic Thermo-Elastic Inputs

EE TPS components are strongly anisotropic, i.e., macro-level margins depend on direction-dependent thermal conductivity, CTE, and stiffness, which are governed by tow/bundle geometry, porosity, and matrix state. Multiscale methods now compute these effective properties from micro/meso representations (including void morphology) and propagate them upward [131,132]. A good example is the multiscale micromechanics/FE-driven workflow for a 3D woven TPS material which reports how microstructural representation at successive length scales changes predicted effective anisotropic thermal conductivities and local thermal fields, which are exactly the quantities that drive thermal gradients, thermal stresses, and recession uncertainty in EE sizing. Complementary image-based FE approaches reconstruct realistic C/CCs microstructures from XCT and use two-scale FE to predict effective CTE while explicitly retaining imperfections/voids, which are critical for predicting thermal-stress-driven cracking under EE-like gradients and cycles [203].

4.3.3. Moving-Boundary Recession and Coupled Aerothermodynamics/Material Response

A central EE challenge is that shape change (recession) feeds back into heating, pressure, and shear. So, sustainability/reuse requires trajectory-consistent coupling rather than isolated stress analysis. A representative approach couples CFD gas–surface physics with a thermal/ablation FE solver and uses mesh movement to realize surface recession, demonstrating how geometry evolution affects ablation for a wedge-type leading edge under hypersonic conditions [204].

At the material scale, microstructure-based thermochemical ablation models for C/CCs explicitly link microstructural evolution to predicted recession rates and surface temperature in agreement with experiments, enabling microstructure-informed "what-if" screening of architectures/coatings for longer life, as depicted in Figure 11b–d [205]. For EE system integration, coupled material response/CFD demonstrations (e.g., Mars-entry style analyses) highlight why this two-way coupling is used in certification-oriented workflows: it reduces boundary-condition inconsistency and quantifies how material response and flow co-evolve [206].

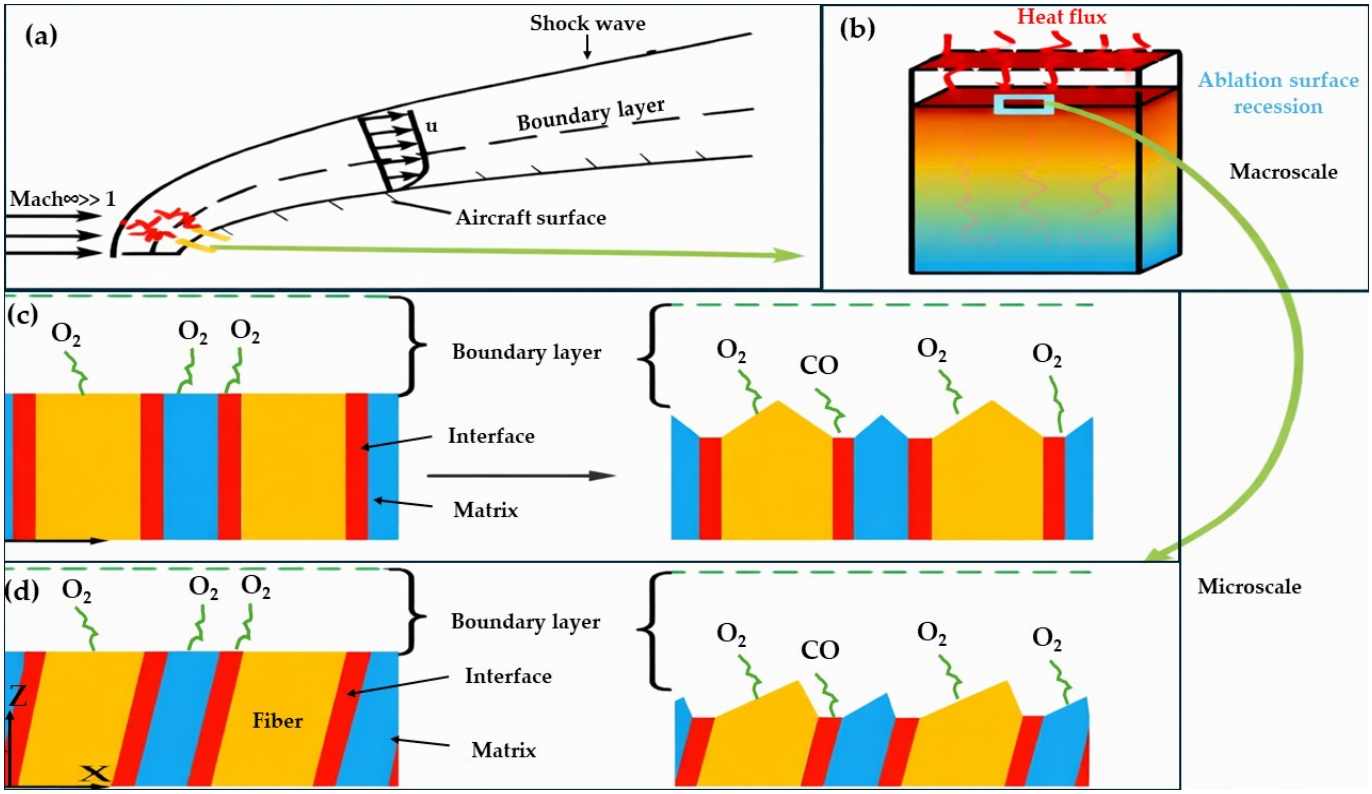

Figure 11. Schematic diagrams of (**a**) hypersonic flow around a bluff body; (**b**) heat transfer and ablation surface recession at the macro-scale; (**c**) changes in the surface morphology of vertical fibers before and after ablation at the micro-scale; and (**d**) changes in the surface morphology of inclined fibers before and after ablation at the micro-scale [205].

5. Challenges and Prospects

This review reinforces that C/CCs remain a uniquely mass-efficient thermostructural platform for extreme aerospace environments, but its long-duration use in oxidizing flows is still limited by a single recurring failure pathway, i.e., oxygen access to carbon through connected defects, whether those defects originate in the substrate (transport porosity) or in protective layers (crack networks). NASA's oxidation studies of SiC-protected C/CCs show that even when the nominal coating chemistry is appropriate, craze cracks and slots in the SiC act as transport pathways, driving subsurface carbon consumption that can be quantified by weight change and X-ray CT scans. The technical implication is that the central durability problem is not "adding a coating but engineering a protection system whose microstructure remains non-percolating to oxidants under thermal cycling, gradients, and erosion.

Across the literature surveyed, the most promising modified C/CCs strategies are those that combine (i) stable, oxidation and ablation-resistant hot-face chemistry, with (ii) an architecture that manages mismatch stresses and defect connectivity, and (iii) a manufacturable pathway to low connected porosity. Recent gradient-layer concepts exemplify this direction where a ZrB_2–SiC coating system that incorporates a graded transition layer (ZrB_2–TiB_2–SiC) fabricated via atmospheric plasma spraying and pack cementation was reported to sustain repeated high-temperature ablation exposures while explicitly attributing performance to mismatch-stress relief and the formation of a protective glassy phase with low oxygen diffusivity, i.e., the gradient is not aesthetic but a stress/transport control strategy. Complementing these "barrier-first" coatings, high-entropy boride coatings are emerging as credible candidates for ultra-high-temperature protection because compositional breadth can stabilize protective reaction layers and delay catastrophic surface

breakdown; recent work explicitly suggested high-entropy borides as effective protectants for C/CCs at ultra-high temperatures.

At the component level, the review also highlights an increasingly mature class of C/CC-derived UHTCMCs produced by RMI and related hybrid densification routes. These systems are "heavier per millimeter" because they intentionally close porosity and introduce ceramic phases, but they target a different design objective, i.e., reusability under high heat flux with retained load-bearing capability. A representative example is a 20 mm thick reusable Cf/SiC–ZrC composite with a gradient-structured matrix produced by RMI, reported with quantified density/open porosity and ablation response under $MW \cdot m^{-2}$ heat flux, alongside post-exposure strength retention, and showed an explicit demonstration that microstructure-controlled ceramic modification can shift the design envelope toward reusable thermal–structural components rather than sacrificial protection alone. More broadly, recent synthesis reviews emphasized that RMI is attractive for fabricating high-density continuous-fiber-reinforced UHTC composites, while also documenting practical limitations (e.g., residual metal phases and fiber/matrix compatibility issues) that remain key down-selection constraints.

A consistent materials-design conclusion also emerges regarding thermal conductivity management. In modified C/CC systems, conductivity must be treated as an engineered, directional property because barrier layers, infiltrated phases, and densification routes alter heat-flow pathways and near-surface thermal gradients that control thermal shock, coating cracking, and recession stability. The practical implication is that the most effective designs combine a hot-face region that is chemically stable and structurally continuous with an interior architecture that limits through-thickness heat leak and preserves damage tolerance—often implemented as graded layers or zoned architectures rather than monolithic coatings. The gradient-coating literature supports this view directly by linking cyclic ablation survivability to stress mitigation and stable reacted-layer formation in graded stacks.

From a manufacturability and qualification standpoint, the literature converges on a clear gate criterion, that modified C/CC systems become "selection-ready" only when the process can reproducibly control the same transport pathways that dominate failure, i.e., connected/transport porosity in the substrate and crack connectivity in protective layers, and verify that control using a component-relevant scale. NASA's oxidation-through-crack results provide a direct durability rationale for treating crack connectivity as a primary manufacturing output, not a secondary defect. Likewise, the HEEET program documentation underscores that system maturation depends not only on material concept but also on manufacturing, integration, and workmanship verification at the engineering-test-unit scale, reflecting the broader aerospace reality that repeatability and thorough inspection are as decisive as coupon performance. For modified C/CC infiltration routes (PIP/CVI hybrids or RMI), this translates into reporting and controlling through-thickness infiltration uniformity and residual connected porosity (permeability/CT-based connectivity metrics), while for sprayed/coated barriers it translates into controlling residual stress and crack networks through graded transition layers and process windows that minimize interconnected defects.

The modeling/software coverage in the review is justified because the state of the art is increasingly toolchain-driven, as credible down-selection requires linking microstructure to effective properties such as gas–surface chemistry to evolving morphology and coupled aerothermal environments to internal response and shape change. NASA's PuMA developments demonstrated image-based extraction of effective properties (e.g., anisotropic conductivity, elasticity, tortuosity, permeability), which directly supports the review's emphasis on connected/transport porosity and heat-flow pathway design. The SPARTA work,

implementing an active-site framework for etch-pit formation on carbon microstructures, illustrates how localized oxidation can be represented mechanistically rather than through purely empirical recession rates. At the component scale, Ares couples flow (US3D) and material response (Icarus) provide consistent BCs and shape-change workflows, aligning with the review's central thesis that EE performance is governed by the coupled thermal–chemical–mechanical phenomena.

Finally, the review highlights the principal barriers to field-wide closure. The most mature knowledge base concerns oxidation/transport-driven degradation mechanisms and the need for stress-managed barrier architectures. The most active frontier involves extending the protective performance of C/CCs above ~2000 °C with multicomponent UHTC/HEC matrix/coatings and integrated UHTCMC architectures while establishing robust cyclic validation datasets and uncertainty-aware sizing workflows. Advancing reusable, high-performance modified C/CC systems will therefore require coordinated progress in (i) defect-connectivity control as an explicit design and manufacturing requirement, (ii) standardized reporting of transport porosity and infiltration uniformity, (iii) cyclic coupled validation under representative thermal–chemical–mechanical loading, and (iv) integrated multiscale modeling toolchains that quantify uncertainty and enable credible thickness sizing and down-selection.

Author Contributions: Conceptualization, J.I.H. and O.I.O.; data curation, J.I.H.; writing—original draft preparation, J.I.H.; writing—review and editing, S.D., A.S. and M.M.R.; visualization, J.I.H.; supervision, O.I.O.; project administration, O.I.O.; funding acquisition, O.I.O. All authors have read and agreed to the published version of the manuscript.

Funding: This research received no external funding.

Data Availability Statement: No new data were created or analyzed in this study.

Conflicts of Interest: The authors declare no conflicts of interest.

References

1. Westwood, M.E.; Webster, J.D.; Day, R.J.; Hayes, F.H.; Taylor, R. Review Oxidation Protection for Carbon Fibre Composites. *J. Mater. Sci.* **1996**, *31*, 1389–1397. [CrossRef]
2. Glass, D.; Dirling, R.; Croop, H.; Fry, T.; Frank, G. Materials Development for Hypersonic Flight Vehicles. In Proceedings of the 14th AIAA/AHI Space Planes and Hypersonic Systems and Technologies Conference, Canberra, Australia, 6–9 November 2006.
3. Peters, A.B.; Zhang, D.; Chen, S.; Ott, C.; Oses, C.; Curtarolo, S.; McCue, I.; Pollock, T.; Prameela, S.E. Materials Design for Hypersonics. *Nat. Commun.* **2024**, *15*, 3328. [CrossRef]
4. Fahrenholtz, W.G.; Hilmas, G.E. Ultra-High Temperature Ceramics: Materials for Extreme Environments. *Scr. Mater.* **2017**, *129*, 94–99. [CrossRef]
5. Agarwal, N.; Rangamani, A.; Bhavsar, K.; Virnodkar, S.S.; Fernandes, A.A.A.; Chadha, U.; Srivastava, D.; Patterson, A.E.; Rajasekharan, V. An Overview of Carbon-Carbon Composite Materials and Their Applications. *Front. Mater.* **2024**, *11*, 1374034. [CrossRef]
6. Binner, J.; Porter, M.; Baker, B.; Zou, J.; Venkatachalam, V.; Diaz, V.R.; D'Angio, A.; Ramanujam, P.; Zhang, T.; Murthy, T.S.R.C. Selection, Processing, Properties and Applications of Ultra-High Temperature Ceramic Matrix Composites, UHTCMCs–a Review. *Int. Mater. Rev.* **2020**, *65*, 389–444. [CrossRef]
7. Venkatapathy, E.; Gasch, M.; Stackpoole, M.; Suman, M.; Morgan, J. Robust and Mass Efficient Thermal Protection Systems for Future Venus Missions. 2021. Available online: https://ntrs.nasa.gov/citations/20210023102 (accessed on 27 April 2026).
8. Feldman, J.D.; Venkatapathy, E.; Mercer, K.J. Development of an Ablative 3D Quartz/Cyanate Ester Composite for the Orion Spacecraft Compression Pad. 2013. Available online: https://ntrs.nasa.gov/citations/20190002016 (accessed on 27 April 2026).
9. Stackpoole, M.; Gasch, M.; Venkatapathy, E.; Violette, S. Development of Lyocell Based Phenolic Impregnated Carbon Ablator (PICA-D) for Future NASA Missions PICA-D and Three Exciting NASA Missions. 2019. Available online: https://ntrs.nasa.gov/citations/20190028255 (accessed on 27 April 2026).
10. Ellerby, D.; Venkatapathy, E.; Gage, P.; Stackpoole, M.; Gasch, M.; Peterson, K.; Young, Z.; Kazemba, C.; Mahzari, M.; Nishioka, O.; et al. Heatshield for Extreme Entry Environment Technology (Heeet) Thermal Protection System (TPS). 2022. Available online: https://ntrs.nasa.gov/api/citations/20190031968/downloads/20190031968.pdf (accessed on 27 April 2026).

11. Chu, Y.; Li, H.; Fu, Q.; Wang, H.; Hou, X.; Zou, X.; Shang, G. Oxidation Protection of C/C Composites with a Multilayer Coating of SiC and Si + SiC + SiC Nanowires. *Carbon* **2012**, *50*, 1280–1288. [CrossRef]
12. National Aeronautics and Space Administration. NASA Facts. 2006. Available online: https://skybrary.aero/articles/national-aeronautics-and-space-administration-nasa (accessed on 27 April 2026).
13. Budelmann, D.; Gibhardt, D.; Fiedler, B. A Review on Aging Effects of Thermoset Prepregs. *Compos. Part B Eng.* **2025**, *303*, 112611. [CrossRef]
14. Rahman, M.A.; Karunarathna, M.S.; Bowland, C.C.; Yang, G.; Gainaru, C.; Li, B.; Kim, S.; Chawla, V.; Ghezawi, N.; Meyer, H.M.; et al. Tough and Recyclable Carbon-Fiber Composites with Exceptional Interfacial Adhesion via a Tailored Vitrimer-Fiber Interface. *Cell Rep. Phys. Sci.* **2023**, *4*. [CrossRef]
15. Heuss, R.; Müller, N.; van Sintern, W.; Starke, A.; Tschiesner, A. *Lightweight, Heavy Impact*; McKinsey & Company: New York, NY, USA, 2012.
16. Maahs, H.G.; Vaughn, W.L. *Four Advances in Carbon-Carbon Materials Technology*; N94-30481; NASA: Washington, DC, USA, 2019.
17. Toro, N.; Okoli, O.I.; Wang, H.P. In-Mold Coating of Composites Manufactured by Resin Infusion between Double Flexible Tooling Process. *J. Reinf. Plast. Compos.* **2005**, *24*, 725–733. [CrossRef]
18. Thagard, J.R.; Okoli, O.I.; Liang, Z. Resin Infusion between Double Flexible Tooling: Evaluation of Process Parameters. *J. Reinf. Plast. Compos.* **2004**, *23*, 1767–1778. [CrossRef]
19. Nwabuzor, A.O.; Okoli, O.I. Preliminary Assessment of the Ultra Violet Curing of Composites Manufactured by the Resin Infusion between Double Flexible Tooling Process. *Polym. Compos.* **2006**, *27*, 417–424. [CrossRef]
20. Caldwell, A.; Feldman, J. Reusable TPS Past, Present, & Future EDL Seminar Series. 2023. Available online: https://ntrs.nasa.gov/api/citations/20230009259/downloads/EDL%20Seminar%20-%20Reusable%20TPS%20Past%20Present%20and%20Future%20v4.0.pdf (accessed on 27 April 2026).
21. Johnson, S.M.; Beach, D. Thermal Protection Materials and Systems: Past and Future. In *Proceedings of the 40th International Conference and Exposition on Advanced Ceramics and Composites*; NASA: Washington, DC, USA, 2015.
22. Sepka, S.A.; Samareh, J.A. Thermal Protection System Mass Estimating Relationships for Blunt-Body, Earth Entry Spacecraft. In Proceedings of the 45th AIAA Thermophysics Conference, Dallas, TX, USA, 22 June 2015.
23. Venakatapathy, E.; Ellerby, D.; Gage, P. Enabling Future Venus In-Situ Missions-Heat-Shield for Extreme Entry Environment Technology (HEEET) Progress Towards TRL 6. 2018. Available online: https://ntrs.nasa.gov/citations/20180007839 (accessed on 27 April 2026).
24. Johnson, S.M. Thermal Protection Materials: Development, Characterization and Evaluation. 2012. Available online: https://ntrs.nasa.gov/api/citations/20120016878/downloads/20120016878.pdf (accessed on 27 April 2026).
25. Wagner, E.B. Research Flights on Blue Origin's New Shepard. *Gravitational Space Res.* **2021**, *9*, 62–67. [CrossRef]
26. Wuchina, E.; Opila, E.; Opeka, M.; Fahrenholtz, W.; Talmy, I. UHTCs: Ultra-High Temperature Ceramic Materials for Extreme Environment Applications. *Electrochem. Soc. Interface* **2007**, *16*, 30–36. [CrossRef]
27. Johnson, S.M.; Gov, S.M.J. Ultra High Temperature Ceramics: Application, Issues and Prospects. 2011. Available online: https://ceramics.org/wp-content/uploads/2011/08/applicatons-uhtc-johnson.pdf (accessed on 27 April 2026).
28. Levine, S.R.; Opila, E.J.; Robinson, R.C.; Lorincz, J.A. Characterization of an Ultra-High Temperature Ceramic Composite. 2004. Available online: https://ntrs.nasa.gov/api/citations/20040074335/downloads/20040074335.pdf (accessed on 27 April 2026).
29. Sciti, D.; Vinci, A.; Zoli, L.; Galizia, P.; Mor, M.; Fahrenholtz, W.; Mungiguerra, S.; Savino, R.; Caporale, A.M.; Airoldi, A. Elevated Temperature Performance: Arc-Jet Testing of Carbon Fiber Reinforced ZrB2 Bars up to 2200 °C for Strength Retention Assessment. *J. Adv. Ceram.* **2025**, *14*, 9221022. [CrossRef]
30. Zhang, H.; Akhtar, F. Refractory Multicomponent Boron-Carbide High Entropy Oxidation-Protective Coating for Carbon-Carbon Composites. *Surf. Coat. Technol.* **2021**, *425*, 127697. [CrossRef]
31. Zhu, S.; Zhang, G.; Bao, Y.; Sun, D.; Zhang, Q.; Meng, X.; Hu, Y.; Yan, L. Progress in Preparation and Ablation Resistance of Ultra-High-Temperature Ceramics Modified C/C Composites for Extreme Environment. *Rev. Adv. Mater. Sci.* **2023**, *62*, 20220276. [CrossRef]
32. Shu, H.; Zhong, W.; Zhao, H.; Hong, F.; Yue, B. Mechanical Properties and High-Pressure Behavior of High Entropy Carbide (Mo, Nb, Ta, V, W)C. *Int. J. Refract. Met. Hard Mater.* **2024**, *121*, 106651. [CrossRef]
33. Demirskyi, D.; Borodianska, H.; Suzuki, T.S.; Sakka, Y.; Yoshimi, K.; Vasylkiv, O. High-Temperature Flexural Strength Performance of Ternary High-Entropy Carbide Consolidated via Spark Plasma Sintering of TaC, ZrC and NbC. *Scr. Mater.* **2019**, *164*, 12–16. [CrossRef]
34. Harrington, T.J.; Gild, J.; Sarker, P.; Toher, C.; Rost, C.M.; Dippo, O.F.; McElfresh, C.; Kaufmann, K.; Marin, E.; Borowski, L.; et al. Phase Stability and Mechanical Properties of Novel High Entropy Transition Metal Carbides. *Acta Mater.* **2019**, *166*, 271–280. [CrossRef]
35. Fu, S.; Jia, Z.; Wan, D.; Bao, Y. Synthesis, Microstructure and Thermophysical Properties of $(La_{0.2}Y_{0.2}Sm_{0.2}Eu_{0.2}Gd_{0.2})_2Zr_2O_7$ High-Entropy Oxide Ceramic. *Ceram. Int.* **2024**, *50*, 5510–5515. [CrossRef]

36. Zhang, D.; Wang, N.; Song, R.; Zhou, M.; Tang, X.; Zhang, Y. A New TBC Material: $(La_{0.2}Gd_{0.2}Y_{0.2}Sm_{0.2}Ce_{0.2})_2Zr_2O_7$ High-Entropy Oxide. *Ceram. Int.* **2024**, *50*, 2490–2500. [CrossRef]
37. Kirnbauer, A.; Spadt, C.; Koller, C.M.; Kolozsvári, S.; Mayrhofer, P.H. High-Entropy Oxide Thin Films Based on Al–Cr–Nb–Ta–Ti. *Vacuum* **2019**, *168*, 108850. [CrossRef]
38. Wright, A.J.; Wang, Q.; Huang, C.; Nieto, A.; Chen, R.; Luo, J. From High-Entropy Ceramics to Compositionally-Complex Ceramics: A Case Study of Fluorite Oxides. *J. Eur. Ceram. Soc.* **2020**, *40*, 2120–2129. [CrossRef]
39. Dippo, O.F.; Mesgarzadeh, N.; Harrington, T.J.; Schrader, G.D.; Vecchio, K.S. Bulk High-Entropy Nitrides and Carbonitrides. *Sci. Rep.* **2020**, *10*, 21288. [CrossRef]
40. Dong, Y.; Zhao, Y.; Li, J.; Chen, J.; Zheng, J.; Sun, D.; Zhang, S.; Wang, S. Super-Hard and Well-Tough (TiZrVCrCoNi)Nx High Entropy Nitride Coatings with Biphasic Nanocomposite Structure. *Vacuum* **2024**, *224*, 113110. [CrossRef]
41. Liu, J.; Zhang, X.; Pelenovich, V.; Xu, Y.; Tan, K.; Hu, L.; Zeng, X.; Zeng, Z.; Lei, Y.; Chen, Y.; et al. Effects of Duty Cycle on Microstructure and Mechanical Properties of (AlCrNbSiTi)N High-Entropy Nitride Hard Coatings Deposited by Pulsed Arc Ion Plating. *Vacuum* **2024**, *225*, 113219. [CrossRef]
42. Chen, R.; Cai, Z.; Pu, J.; Lu, Z.; Chen, S.; Zheng, S.; Zeng, C. Effects of Nitriding on the Microstructure and Properties of VAlTiCrMo High-Entropy Alloy Coatings by Sputtering Technique. *J. Alloys Compd.* **2020**, *827*, 153836. [CrossRef]
43. Pakhomova, E.; Cao, G.; Orrù, R.; Garroni, S.; Ferro, P.; Licheri, R. High-Entropy Diborides—Silicon Carbide Composites by Reactive and Non-Reactive Spark Plasma Sintering: A Comparative Study. *Materials* **2024**, *17*, 718. [CrossRef]
44. Feng, L.; Fahrenholtz, W.G.; Hilmas, G.E.; Monteverde, F. Effect of Nb Content on the Phase Composition, Densification, Microstructure, and Mechanical Properties of High-Entropy Boride Ceramics. *J. Eur. Ceram. Soc.* **2021**, *41*, 92–100. [CrossRef]
45. Zhang, Y.; Jiang, Z.B.; Sun, S.K.; Guo, W.M.; Chen, Q.S.; Qiu, J.X.; Plucknett, K.; Lin, H.T. Microstructure and Mechanical Properties of High-Entropy Borides Derived from Boro/Carbothermal Reduction. *J. Eur. Ceram. Soc.* **2019**, *39*, 3920–3924. [CrossRef]
46. Shen, X.Q.; Liu, J.X.; Li, F.; Zhang, G.J. Preparation and Characterization of Diboride-Based High Entropy $(Ti_{0.2}Zr_{0.2}Hf_{0.2}Nb_{0.2}Ta_{0.2})B_2$–SiC Particulate Composites. *Ceram. Int.* **2019**, *45*, 24508–24514. [CrossRef]
47. Du, B.; Cheng, Y.; Xun, L.; Zhang, S.; Tong, J.; Lv, Q.; Zhou, S.; Hu, P.; Zhang, X. Using PyC Modified 3D Carbon Fiber to Reinforce UHTC under Low Temperature Sintering without Pressure. *J. Adv. Ceram.* **2021**, *10*, 871–884. [CrossRef]
48. Zhang, C.; Hu, P.; Xun, L.; Zhou, Y.; Han, J.; Zhang, X. A Universal Strategy towards the Fabrication of Ultra-High Temperature Ceramic Matrix Composites with Outstanding Mechanical Properties and Ablation Resistance. *Compos. B Eng.* **2024**, *280*, 111485. [CrossRef]
49. Zhao, S.; Yang, Z.C.; Zhou, X.G. Fracture Behavior of SiC/SiC Composites with Different Interfaces. *Wuji Cailiao Xuebao/J. Inorg. Mater.* **2016**, *31*, 58–62. [CrossRef]
50. Rubio, V.; Ramanujam, P.; Cousinet, S.; LePage, G.; Ackerman, T.; Hussain, A.; Brown, P.; Dautremonte, I.; Binner, J. Thermal Properties and Performance of Carbon Fiber-Based Ultra-High Temperature Ceramic Matrix Composites (Cf-UHTCMCs). *J. Am. Ceram. Soc.* **2020**, *103*, 3788–3796. [CrossRef]
51. Sziroczak, D.; Smith, H. A Review of Design Issues Specific to Hypersonic Flight Vehicles. *Prog. Aerosp. Sci.* **2016**, *84*, 1–28. [CrossRef]
52. Luo, R.; Liu, T.; Li, J.; Zhang, H.; Chen, Z.; Tian, G. Thermophysical Properties of Carbon/Carbon Composites and Physical Mechanism of Thermal Expansion and Thermal Conductivity. *Carbon* **2004**, *42*, 2887–2895. [CrossRef]
53. Mitchell, D.; Tiley, J. History and State of the Art in Advanced Thermal Protection Systems. 2024. Available online: https://info.ornl.gov/sites/publications/Files/Pub217821.pdf (accessed on 27 April 2026).
54. Opeka, M.M.; Talmy, I.G.; Wuchina, E.J.; Zaykoski, J.A.; Causey, S.J. Mechanical, Thermal, and Oxidation Properties of Refractory Hafnium and Zirconium Compounds. *J. Eur. Ceram. Soc.* **1999**, *19*, 2405–2414. [CrossRef]
55. Mahzari, M.; Milos, F. Sizing and Margin Methodology for Dual-Layer Thermal Protection Systems. 2018. Available online: https://pdfs.semanticscholar.org/8a17/5afaa2c73438da7756de4edd6f9030b96547.pdf (accessed on 27 April 2026).
56. Narottam, P. Bansal Handbook of Ceramic Composites. 2005. Available online: https://content.e-bookshelf.de/media/reading/L-398-a05c1440bf.pdf (accessed on 27 April 2026).
57. Baltimore, S.; Glass, D.E. Hypersonic Materials and Structures. 2016. Available online: https://ntrs.nasa.gov/citations/20160007098 (accessed on 27 April 2026).
58. Su, L.; Li, B.; Wang, H.; Niu, M.; Fan, X. SiOC Modified Carbon-Bonded Carbon Fiber Composite with SiC Nanowires Enhanced Interfibrous Junctions. *J. Am. Ceram. Soc.* **2020**, *103*, 3321–3329. [CrossRef]
59. Zhang, F.; Cui, W.; Wang, B.; Xu, B.; Liu, X.; Liu, X.; Jia, Z.; Wu, G. Morphology-Control Synthesis of Polyaniline Decorative Porous Carbon with Remarkable Electromagnetic Wave Absorption Capabilities. *Compos. B Eng.* **2021**, *204*, 108491. [CrossRef]
60. Feng, G.; Li, H.; Yao, X.; Zhou, H.; Yu, Y.; Lu, J. Ablation Resistance of HfC-TaC/HfC-SiC Alternate Coating for SiC-Coated Carbon/Carbon Composites under Cyclic Ablation. *J. Eur. Ceram. Soc.* **2021**, *41*, 3207–3218. [CrossRef]

61. Fang, C.; Huang, B.; Yang, X.; Shi, A.; Zhang, Z.; Yi, J.; Huang, Q. Effects of LaB6 on Composition, Microstructure and Ablation Property of the HfC-TaC-SiC Doped C/C Composites Prepared by Precursor Infiltration and Pyrolysis. *Corros. Sci.* **2021**, *184*, 109347. [CrossRef]
62. HEEET Project. Overview of Mission Sizing For Heatshield for Extreme Entry Environments Technology (HEEET) Materials Overview of Mission Sizing for Heatshield for Extreme Entry Environments Technology (HEEET) Materials. 2014. Available online: https://discovery.larc.nasa.gov/pdf_files/26_HEEET_Mission_TPS_Sizing_Summary_(HEEET-1004).pdf (accessed on 27 April 2026).
63. Wright, M.J.; Wercinski, P.F.; Munk, M.M.; Dutta, S.; Rickman, S.L.; Powell, R.W.; Austin, A.; Nelessen, A.; Lobia, M.; Arc, N.; et al. Thermal Protection System to Enable Ice Giant Aerocapture Mission for Delivering Both an Orbiter and an in Situ Probe. 2020. Available online: https://ntrs.nasa.gov/api/citations/20205007310/downloads/White%20Paper_Aerocapture%20TPS_Final.pdf (accessed on 27 April 2026).
64. Ohlhorst, C.W.; Glass, D.E.; Bruce, W.; Lindell, M.; Vaughn, W.L.; Smith, R.; Dirling, R.B., Jr.; Hogenson, P.A.; Nichols, J.M.; Thompson, D.R.; et al. Cleared for Public Release Development of X-43A Mach 10 Leading Edges. 2005. Available online: https://www.semanticscholar.org/paper/Cleared-for-Public-Release-DEVELOPMENT-OF-X-43-A-10-Ohlhorst-Glass/2ae8560b40b9006bbe3fc94a47e30de50de65063 (accessed on 27 April 2026).
65. Guo, G.; Ye, F.; Cheng, L.; Wei, Y.; Chen, X. Ablation and Mechanical Behavior of Reusable Cf/SiC-ZrC with a Gradient-Structured Matrix Produced by Reactive Melt Infiltration. *Carbon* **2024**, *229*, 119504. [CrossRef]
66. Morgan, J.; Venkatapathy, E.; Gasch, M.; Williams, J.; Deshmukh, R.G.; Shellabarger, E.; Scoggins, J.B.; Gomez-Delrio, A.; Dutta, S. Thermal Protection System Design of Aerocapture Systems for Uranus Orbiters. In Proceedings of the AIAA SCITECH 2024 Forum, Orlando, FL, USA, 8–12 January 2024.
67. Sepka, S.; Gasch, M.; Beck, R.A.; White, S. Testing of Candidate Rigid Heat Shield Materials at LHMEL for the Entry, Descent, and Landing Technology Development Project. 2012. Available online: https://scispace.com/pdf/testing-of-candidate-rigid-heat-shield-materials-at-lhmel-286iut2e03.pdf (accessed on 27 April 2026).
68. Blette, D.J.; Sidor, A.T.; Theisinger, J.E.; Omidy, A.D. Overview of Additively Manufactured TPS Proposed Flight Test and Earth Re-Entry Capsule Design. 2024. Available online: https://ntrs.nasa.gov/api/citations/20230013631/downloads/AMTPS_Main.pdf (accessed on 27 April 2026).
69. Zhang, Y.; Zhang, X.; Ou, H.; Wang, B.; Sun, J.; Fu, Q. Heat Dissipation of Carbon Shell in ZrC–SiC/TaC Coating to Improve Protective Ability against Ultrahigh Temperature Ablation. *J. Adv. Ceram.* **2024**, *13*, 1080–1091. [CrossRef]
70. Wu, M.; Liu, Y.; Qu, W.; Guo, W.; Zhang, H.; Pei, Y.; Li, S.; Gong, S. Thickness-Related Failure Behaviors of the Thermal Barrier Coatings under Thermal Gradient Cycling. *Surf. Coat. Technol.* **2023**, *468*, 129748. [CrossRef]
71. Lv, J.; Li, W.; Li, T.; Gao, B.; Li, J.; Fu, Y.; Guo, L.; Zhang, Y. Multicomponent (Hf-Zr-Ta)B2 Coatings for Carbon/Carbon Composites and Structural Optimization Enabling Superior Ablation Resistance. *J. Mater. Sci. Technol.* **2025**, *204*, 115–126. [CrossRef]
72. Li, J.; Zhang, Y.; Zhao, Y.; Zou, Y.; Lv, J.; Li, J. A Novel $(Hf_{1/3}Zr_{1/3}Ti_{1/3})C$ Medium-Entropy Carbide Coating with Excellent Long-Life Ablation Resistance Applied above 2100 °C. *Compos. Part B Eng.* **2023**, *251*, 110467. [CrossRef]
73. Liu, Z.; Wang, Y.; Xiong, X.; Ye, Z.; Long, Q.; Wang, J.; Li, T.; Liu, C. Microstructure and Ablation Behavior of C/C-SiC-$(Zr_xHf_{1-x})C$ Composites Prepared by Reactive Melt Infiltration Method. *Materials* **2023**, *16*, 2120. [CrossRef] [PubMed]
74. Tülbez, S. Processing and Characterization of Carbon Fiber Reinforced Silicon Carbide (C/C-SiC) Matrix Composites a Thesis Submitted to the Graduate School of Natural and Applied Sciences of Middle East Technical University. 2015. Available online: https://etd.lib.metu.edu.tr/upload/12618944/index.pdf (accessed on 27 April 2026).
75. Wan, F.; Pizada, T.J.; Liu, R.; Wang, Y.; Qi, G.; Zhang, C.; Marrow, T.J. Structure and Flexural Properties of 3D Needled Carbon Fiber Reinforced Carbon and Silicon Carbide (C/C-SiC) Composites Fabricated by Gaseous and Liquid Silicon Infiltration. *Ceram. Int.* **2019**, *45*, 17978–17986. [CrossRef]
76. Sun, Q.; Zhang, H.; Huang, C.; Zhang, W. Fabrication of C/C–SiC–ZrB2 Ultra-High Temperature Composites through Liquid–Solid Chemical Reaction. *Crystals* **2021**, *11*, 1352. [CrossRef]
77. Tang, Z.; Yi, M.; Xiang, Q.; Du, Y.; Peng, K. Mechanical and Ablation Properties of a C/C-HfB2-SiC Composite Prepared by High-Solid-Loading Slurry Impregnation Combined with Precursor Infiltration and Pyrolysis. *J. Eur. Ceram. Soc.* **2021**, *41*, 6160–6170. [CrossRef]
78. Kolodziej, P. *Aerothermal Performance Constraints for Hypervelocity Small Radius Unswept Leading Edges and Nosetips*; NASA Technical Memorandum 112204; NASA: Washington, DC, USA, 1997.
79. Ohlhorst, C.W.; Vaughn, W.L.; Ransone, P.O. Thermal Conductivity Database of Various Structural Carbon-Carbon Composite Materials. 1997. Available online: https://ntrs.nasa.gov/citations/19970041399 (accessed on 27 April 2026).
80. Li, B.; Zhu, C.; Xu, H.; Qin, Y.; Shan, C.; Gao, F.; Guo, J.; Dong, Z.; Li, X. The Microstructure and Thermal Conductive Behavior of Three-Dimensional Carbon/Carbon Composites with Ultrahigh Thermal Conductivity. *Materials* **2024**, *17*, 983. [CrossRef]

81. Zhao, Y.; Yan, K.; Song, Q.; Xiao, C.; Jiao, Y.; Shen, Q.; Li, H. A New Strategy to Improve the Ablation Resistance of C/C-ZrC-SiC Composites by Using Mesophase-Pitch-Based Carbon Fibers as Heat Transfer Channels. *Ceram. Int.* **2025**, *51*, 10103–10114. [CrossRef]
82. Huang, D.; Liu, Q.; Zhang, Y.; Ye, C.; Zhu, S.; Fan, Z.; Han, F.; Liu, H.; Liu, J. Ablation Behavior and Thermal Conduction Mechanism of 3D ZrC–SiC-Modified Carbon/Carbon Composite Having High Thermal Conductivity Using Mesophase-Pitch-Based Carbon Fibers and Pyrocarbon as Heat Transfer Channels. *Compos. Part B Eng.* **2021**, *224*, 109201. [CrossRef]
83. Wang, S.; Yin, J.; Xiefeng, M.; Tang, L.; Xiong, X.; Zhang, H.; Wen, Q.; Ma, D.; Zuo, J. Microstructure and Ablation Behaviour of C/C-SiC-ZrC-Cu Composites Prepared by Reactive Melt Infiltration. *Mater. Today Commun.* **2024**, *38*, 108389. [CrossRef]
84. Wang, R.; Zhang, J.; Zhang, J.; Li, B.; Tan, C.; Yang, X.; Bai, L.; Fei, J.; Fu, Q. Gradient Structured C/C-ZrC-SiC Composites with Enhanced Mechanical and Ablation Properties. *Ceram. Int.* **2025**, *51*, 17774–17785. [CrossRef]
85. Liu, F.; Li, H.; Fu, Q.; He, X.; Zhang, W. $ZrSi_2$-SiC/SiC Gradient Coating of Micro-Structure and Anti-Oxidation Property on C/C Composites Prepared by SAPS. *Coatings* **2022**, *12*, 1377. [CrossRef]
86. Cairo, C.A.A.; Graça, M.L.A.; Silva, C.R.M.; Bressiani, J.C. Functionally Gradient Ceramic Coating for Carbon–Carbon Antioxidation Protection. *J. Eur. Ceram. Soc.* **2001**, *21*, 325–329. [CrossRef]
87. Xue, C.; Zhou, H.; Hu, J.; Wang, H.; Xu, J.; Dong, S. Fabrication and Microstructure of ZrB2–ZrC–SiC Coatings on C/C Composites by Reactive Melt Infiltration Using ZrSi2 Alloy. *J. Adv. Ceram.* **2018**, *7*, 64–71. [CrossRef]
88. Feng, S.; Dai, W.; Yang, X.; Zhu, S.; Zuo, H.; Chen, H.; Yang, T.; Liu, W.; Pei, Y. Study on the Gradient Characteristics of Reactive Melt Infiltration C/SiC-HfC Composite. *Mater. Lett.* **2024**, *370*, 136823. [CrossRef]
89. Liu, S.; Wang, Y.; Gu, P.; Ma, Z.; Liu, Y.; Zhu, S. Fabrication and Ablation Behavior of ZrB2-SiC/ZrB2-TiB2-SiC Gradient Coating on Carbon/Carbon Composites. *J. Alloys Compd.* **2025**, *1038*, 182734. [CrossRef]
90. Hu, D.; Fu, Q.; Liu, T.; Tong, M. Structural Design and Ablation Performance of ZrB2/MoSi2 Laminated Coating for SiC Coated Carbon/Carbon Composites. *J. Eur. Ceram. Soc.* **2020**, *40*, 212–219. [CrossRef]
91. Liu, G.; Cheng, L.; Luan, X.; Zhang, J. Damage Behavior of Atomic Oxygen on CVD SiC Coating-Modified Carbon/Carbon Composite in Low Earth Orbit Environment. *J. Mater. Sci. Technol.* **2019**, *35*, 2957–2965. [CrossRef]
92. Jian, K.; Chen, Z.H.; Ma, Q.S.; Zheng, W.W. Effects of Pyrolysis Processes on the Microstructures and Mechanical Properties of Cf/SiC Composites Using Polycarbosilane. *Mater. Sci. Eng. A* **2005**, *390*, 154–158. [CrossRef]
93. Patterson, M.C.L.; He, S.; Fehrenbacher, L.L.; Hanigofsky, J.; Reed, B.D. Advanced HfC-TaC Oxidation Resistant Composite Rocket Thruster. *Mater. Manuf. Process.* **1996**, *11*, 367–379. [CrossRef]
94. Guo, R.; Li, Z.; Li, L.; Zheng, R.; Ma, C. Oxidation Behavior of High-Entropy $(Zr_{0.2}Hf_{0.2}Ta_{0.2}Nb_{0.2}Ti_{0.2})B_2$ Ceramic with 20% SiC Addition. *J. Eur. Ceram. Soc.* **2024**, *44*, 5181–5189. [CrossRef]
95. Jacobson, N.S.; Roth, D.J.; Rauser, R.W.; Curry, D.M.; Cawley, J.D.; Curry, D.M. Oxidation Through Coating Cracks of SiC-Protected Carbon/Carbon. *Surf. Coat. Technol.* **2008**, *203*, 372–383. [CrossRef]
96. Li, J.; Zhang, Y.; Lv, J.; Li, T.; Zhu, X.; Gai, W. Sealing Role of Ti-Rich Phase in HfC-ZrC-TiC Coating for C/C Composites during Ablation above 2100 °C. *Corros. Sci.* **2022**, *205*, 110474. [CrossRef]
97. Tang, Z.; Zhou, Y.; Liu, R.; Yi, M.; Peng, K. Preparation and Ablation Behavior of a ZrB2-SiC Coating-Matrix Integrated C/C Composite. *J. Eur. Ceram. Soc.* **2024**, *44*, 2998–3011. [CrossRef]
98. Ward, T.Z.; Wilkerson, R.P.; Musicó, B.L.; Foley, A.; Brahlek, M.; Weber, W.J.; Sickafus, K.E.; Mazza, A.R. High Entropy Ceramics for Applications in Extreme Environments. *J. Phys. Mater.* **2024**, *7*, 021001. [CrossRef]
99. Xu, J.; Guo, L.; Kong, J.; Ma, Y.; Wang, H.; Wang, J. The Mechanical Properties of C/C-ZrC-SiC Composites after Laser Ablation. *J. Eur. Ceram. Soc.* **2023**, *43*, 6732–6745. [CrossRef]
100. Sun, J.; Li, X.; Zhao, L.; Du, Q.; Zhao, J. Simultaneously Enhancing the Toughness and Strength of Cemented TiB2 Nanocomposites through Doping SiC Whisker and Graphene. *J. Mater. Res. Technol.* **2023**, *26*, 9509–9517. [CrossRef]
101. Zhang, T.; Xu, H.; Zhang, C.; Zhang, Y.; Chi, Q. Investigation of Electrical and Mechanical Properties of Silicon Carbide Whisker-Hexagonal Boron Nitride/Ethylene Propylene Diene Monomer Composites. *J. Mater. Sci. Mater. Electron.* **2023**, *34*, 1451. [CrossRef]
102. Lu, D.; Cheng, S.; Jin, L.; Zhang, L.; Shi, D.; Yue, H.; Zeng, T. Effect of Temperature on SiC Whiskers Growth of SiCw/SiC Composites Based on Selective Laser Sintering and Their Mechanical Properties. *J. Alloys Compd.* **2023**, *938*, 168624. [CrossRef]
103. Mao, F.; Huang, X.; Ma, X.; Yang, X.; Zhang, X.; Yan, Q. Microstructure Evolutions of SiC Whiskers at High Temperature and Its Effects on Silicon Carbide Ceramics. *Ceram. Int.* **2023**, *49*, 29584–29594. [CrossRef]
104. Su, Y.; Yang, Y.; Zhu, T.; Wang, H.; Liang, X.; Li, Y.; Xie, Z.; Han, Y. Microstructure and Mechanical Properties of SiC-GNPS-SiCW Ceramics by Oscillatory Pressure Sintering. *Ceram. Int.* **2024**, *50*, 10392–10401. [CrossRef]
105. Zhang, Z.; Liu, H.; Zhang, Z.; Han, G.; Sun, X.; Li, N.; Yuan, C.; Wang, W.; Zhang, W. SiC Whisker Toughened WC-Al2O3-ZrO2 Binderless Cemented Carbides via Fast-Hot-Pressed Sintering and DFT Calculations. *Ceram. Int.* **2024**. [CrossRef]
106. Zeng, Y.; Zhang, J.; Hou, J.; Wang, Y.; Li, H. Improved Oxidation and Thermal Shock Resistance of SiC-Si Coating with a SiCw/PyC Network Structure Toughened Buffer Layer. *Surf. Coat. Technol.* **2024**, *479*, 130522. [CrossRef]

107. Yan, T.; Luo, M.; Chen, J.; Zhu, H.; Chai, J.; Niu, L.; Chen, B.; Zhu, Y.; Shen, T. Microstructure and Mechanical Properties of High Entropy (MoTaTiVW)C5 Ceramics Toughened with Silicon Carbide Whisker. *Ceram. Int.* **2024**, *50*, 15840–15847. [CrossRef]
108. Fu, Q.; Sui, S.; Ma, Y.; Sun, S.; Wang, X.; Meng, Q.; Li, S.; Zhao, Y. Silicon Carbide Whiskers Reinforced Silicon Carbide Ceramics Prepared by Vat Photopolymerization and Liquid Silicon Infiltration. *Ceram. Int.* **2024**, *50*, 17747–17755. [CrossRef]
109. Zhao, Z.; Li, K.; Li, W.; Liu, Q.; Kou, G.; Zhang, Y. Ablation Behavior of C/C-ZrC-SiC Composites Prepared by Reactive Melt Infiltration under Oxyacetylene Torch at Two Heat Fluxes. *Ceram. Int.* **2018**, *44*, 17345–17358. [CrossRef]
110. Tang, S.; Deng, J.; Wang, S.; Liu, W. Fabrication and Characterization of an Ultra-High-Temperature Carbon Fiber-Reinforced ZrB2-SiC Matrix Composite. *J. Am. Ceram. Soc.* **2007**, *90*, 3320–3322. [CrossRef]
111. Wang, Y.; Liu, W.; Cheng, L.; Zhang, L. Preparation and Properties of 2D C/ZrB2-SiC Ultra High Temperature Ceramic Composites. *Mater. Sci. Eng. A* **2009**, *524*, 129–133. [CrossRef]
112. Zeng, Y.; Wang, D.; Xiong, X.; Gao, S.; Chen, Z.; Sun, W.; Wang, Y. Ultra-High-Temperature Ablation Behavior of SiC–ZrC–TiC Modified Carbon/Carbon Composites Fabricated via Reactive Melt Infiltration. *J. Eur. Ceram. Soc.* **2020**, *40*, 651–659. [CrossRef]
113. Song, X.; Zhang, Z.; Ye, L.; Li, W.; Han, W.; Yan, S. Preparation and Ablation Behavior Analysis of Non-Equimolar Cf/$(Hf_{1/2}Zr_{1/3}Ti_{1/6})$C Composites under Oxyacetylene Flame with Different Heat Fluxes. *Ceram. Int.* **2024**, *50*, 26482–26492. [CrossRef]
114. Murthy, S.S.N.; Patel, M.; Reddy, T.S.; Prasad, V.V.B.; Panigrahi, B.B. Processing and Characterization of Carbon Fibres Reinforced ZrB2 Ultra High Temperature Ceramic Matrix Composite. *Ceram. Int.* **2021**, *47*, 32438–32444. [CrossRef]
115. Luo, L.; Wang, Y.; Duan, L.; Liu, L.; Wang, G. Ablation Behavior of C/SiC-HfC Composites in the Plasma Wind Tunnel. *J. Eur. Ceram. Soc.* **2016**, *36*, 3801–3807. [CrossRef]
116. Dong, Z.; Yu, H.; Zhang, Y.; Liu, B.; Zhang, H.; Zhang, J.; Fu, Q. C/C-HfC-ZrC Composites with Excellent Long-Term Ablation Performance Prepared by Combining PIP and RMI. *Ceram. Int.* **2024**, *50*, 13912–13923. [CrossRef]
117. Mor, M.; Vinci, A.; Sciti, D. Processing and Oxidation Resistance at 1650 °C of ZrB2-Based UHTCMCs with Short Fibre Gradients. *J. Eur. Ceram. Soc.* **2024**, *44*, 4536–4548. [CrossRef]
118. Galizia, P.; Vinci, A.; Zoli, L.; Airoldi, A.; Caporale, A.M.; Mungiguerra, S.; Savino, R.; De, M.; Fumo, S.; Sciti, D. Impact of Arc-Jet Tests at 2200 °C and Thermal Vacuum Cycles on Microstructure and Mechanical Behaviour of Cf-ZrB2 UHTCMCs. 2024. Available online: https://scholarsmine.mst.edu/cgi/viewcontent.cgi?article=4853&context=matsci_eng_facwork (accessed on 27 April 2026).
119. Tao, C.; Liao, H.; Chen, B.; Mao, W.; Wang, J.; Dai, C.; Fan, Z.; Zhou, Z.; Zuo, J. Ablation Behavior and Mechanism of (PyC-Csf)/ZrB2-SiC-ZrC Ceramics Sintered by Reactive Spark Plasma Sintering at Low Temperature. *Corros. Sci.* **2024**, *229*, 111873. [CrossRef]
120. Wang, R.; Zhang, J.; Fei, J.; Liu, C.; Fu, Q. Effect of ZrB2 on the Ablation Behavior of Cf/ZrB2-ZrC-SiC Sharp Leading Edge Composites by PIP and RMI. *Mater. Charact.* **2024**, *211*, 113898. [CrossRef]
121. Chen, B.; Ni, D.; Bao, W.; Liao, C.; Luo, W.; Song, E.; Dong, S. Engineering Cf/ZrB_2-SiC-Y_2O_3 for Thermal Structures of Hypersonic Vehicles with Excellent Long-Term Ultrahigh Temperature Ablation Resistance. *Adv. Sci.* **2023**, *10*, e2304254. [CrossRef]
122. Duan, L.; Luo, L.; Liu, L.; Wang, Y. Ablation of C/SiC-HfC Composite Prepared by Precursor Infiltration and Pyrolysis in Plasma Wind Tunnel. *J. Adv. Ceram.* **2020**, *9*, 393–402. [CrossRef]
123. Chen, L.; Wu, Y.; Wang, W.; Yuan, X.; Liu, C.; Li, C. Fabrication and Ablation Properties of SiC Nanowires-Network Modified Carbon/Carbon–Ultrahigh Temperature Ceramics Composites. *J. Compos. Sci.* **2024**, *8*, 108. [CrossRef]
124. Yan, C.; Liu, F.; Wang, W.; Liu, R. Mechanical, Thermophysical, and Ablation Properties of C/HfC–SiC Composites with Various SiC/HfC Ratios. *Int. J. Appl. Ceram. Technol.* **2025**, *22*, e14878. [CrossRef]
125. Liu, Z.; Jia, Y.; Hou, J.; Zhang, R.; Zhang, S.; Zhang, J.; Fu, Q.Q. C/C-HfC-SiC Composites with Simultaneous the Resistance to Ultra-High Temperature Airflow Erosion and High Temperature Oxidation. *J. Mater.* **2025**, *11*, 100846. [CrossRef]
126. Cao, Y.; Lu, J.; Zhou, Z.; Meng, J.; Zhang, R.; Liu, W.; Li, H. Fabrication, Mechanical Properties and Ablation Performance of SiCnw/PyC-C/C-HfC-SiC Composites with a Si-Rich Coating via Film Boiling Chemical Vapor Infiltration and Gaseous Silicon Infiltration. *J. Eur. Ceram. Soc.* **2025**, *45*, 117609. [CrossRef]
127. Xu, C.; Huang, J.; Su, Y.; Jia, C.; Chen, S. High-Thermal-Conductivity C/C-HfC-SiC Composites with Enhanced Ablation Resistance for Oxidative Environments above 3000 °C. *J. Alloys Compd.* **2026**, *1063*, 187608. [CrossRef]
128. Kopeliovich, D. Advances in Manufacture of Ceramic Matrix Composites by Infiltration Techniques. In *Advances in Ceramic Matrix Composites*, 2nd ed.; Elsevier Inc.: Amsterdam, The Netherlands, 2018; pp. 93–119. ISBN 9780081021675.
129. Ekuase, O.A.; Anjum, N.; Eze, V.O.; Okoli, O.I. A Review on the Out-of-Autoclave Process for Composite Manufacturing. *J. Compos. Sci.* **2022**, *6*, 172. [CrossRef]
130. D'Angio, A. Microwave Enhanced Chemical Vapour Infiltration of Silicon Carbide Fibre Preforms. 2018. Available online: https://etheses.bham.ac.uk/id/eprint/8188/1/D'Angio2018PhD.pdf (accessed on 27 April 2026).

131. Bednarcyk, B.A.; Ricks, T.M.; Pineda, E.J.; Murthy, P.L.N.; Mital, S.K.; Hu, Z.; Gustafson, P.A. Thermal Conductivity of 3D Woven Composite Thermal Protection System Materials via Multiscale Recursive Micromechanics. In Proceedings of the AIAA SCITECH 2022 Forum, San Diego, CA, USA, 3–7 January 2022.
132. Kirillov, A.; Mintun, E.; Ravi, N.; Mao, H.; Rolland, C.; Gustafson, L.; Xiao, T.; Whitehead, S.; Berg, A.C.; Lo, W.Y.; et al. Segment Anything. In *Proceedings of the IEEE International Conference on Computer Vision*; Institute of Electrical and Electronics Engineers Inc.: New York, NY, USA, 2023; pp. 3992–4003.
133. Wei, J.; Thukral, A.; Pandey, R.; Bhattacharyya, K.X.; Karki, B.; Cordeiro, J.C., Jr.; Llanes, L.; Iftime, G. Simplified, Infiltration-Free Ceramic Matrix Composite Manufacturing. *SAMPE J.* **2024**, *60*. [CrossRef]
134. Tan, Z.; Zhang, X.; Ruan, J.; Liao, J.; Yu, F.; Xia, L.; Wang, B.; Liang, C. Synthesis, Structure, and Properties of Carbon/Carbon Composites Artificial Rib for Chest Wall Reconstruction. *Sci. Rep.* **2021**, *11*, 11285. [CrossRef]
135. Janicki, J.C.; Egloff, M.C.; Bajwa, D.S.; Amendola, R.; Ryan, C.A.; Cairns, D.S. Design of Experiment to Determine the Effect of the Geometric Variables on Tensile Properties of Carbon Fiber Reinforced Polymer Composites. *J. Compos. Sci.* **2023**, *7*, 222. [CrossRef]
136. Yan, C.; Liu, R.; Zha, B.; Zhang, C. Fabrication and Properties of 3-Dimensional 4-Directional Cf/HfC-SiC Composites by Precursor Impregnation and Pyrolysis Process. *J. Alloys Compd.* **2018**, *739*, 955–960. [CrossRef]
137. Rubio, V.; Binner, J.; Cousinet, S.; Le Page, G.; Ackerman, T.; Hussain, A.; Brown, P.; Dautremont, I. Materials Characterisation and Mechanical Properties of Cf-UHTC Powder Composites. *J. Eur. Ceram. Soc.* **2019**, *39*, 813–824. [CrossRef]
138. Kütemeyer, M.; Schomer, L.; Helmreich, T.; Rosiwal, S.; Koch, D. Fabrication of Ultra High Temperature Ceramic Matrix Composites Using a Reactive Melt Infiltration Process. *J. Eur. Ceram. Soc.* **2016**, *36*, 3647–3655. [CrossRef]
139. Liu, J.C.; Wang, D.Y.; Chen, Y.W.; Li, S.H.; Wei, H.Z. Research on Manufacturing Process of Carbon-Carbon Composites as Ablation Resistance Materials. *Proc. Adv. Mater. Res.* **2013**, *813*, 419–426. [CrossRef]
140. Bendjerad, A.; Boukhtache, S.; Benhaya, A.; Luneau, D.; El Hak Abaidia, S.; Benyahia, K. Modeling of Magnetic Properties of Iron Thin Films Deposited by RF Magnetron Sputtering Using Preisach Model. *Serbian J. Electr. Eng.* **2016**, *13*, 229–238. [CrossRef]
141. Navas, D.; Fuentes, S.; Castro-Alvarez, A.; Chavez-Angel, E. Review on Sol-Gel Synthesis of Perovskite and Oxide Nanomaterials. *Gels* **2021**, *7*, 275. [CrossRef]
142. Shahzad, S.; Iqbal, K.; Uddin, Z. Theoretical Study of Reactive Melt Infiltration to Fabricate Co-Si/C Composites. *Chin. Phys. B* **2021**, *30*, 116102. [CrossRef]
143. Bai, Z.; Cao, L.; Huang, J.; Ouyang, H.; Su, J.; Li, C.; Fu, A. Cf/C-SiC-MoSi2 Composites with Good Ablation Performance Prepared via a Two-Step Hydrothermal Method. *RSC Adv.* **2017**, *7*, 11707–11718. [CrossRef]
144. Kim, J.W.; Lee, J.S. Influence of Interleaved Films on the Mechanical Properties of Carbon Fiber Fabric/Polypropylene Thermoplastic Composites. *Materials* **2016**, *9*, 344. [CrossRef] [PubMed]
145. Fowler, M.E. Process Specification for the Trimming and Drilling of Composites. 2020. Available online: https://www.nasa.gov/wp-content/uploads/2023/03/prc-6003-current.pdf (accessed on 27 April 2026).
146. Mueller, J.; Brown, D.K.; Ganer, C.E.; Brophy, J.R. Fabrication of Carbon-Carbon Grids for Ion Optics. 1993. Available online: https://ntrs.nasa.gov/citations/19920066153 (accessed on 27 April 2026).
147. Johnson, L.B. *National Aeronautics and Space Administration Carbon Structure Hazard Control*; NASA: Washington, DC, USA, 2015.
148. Knight, N.F.; Song, K.; Raju, I.S. Space Shuttle Orbiter Wing-Leading-Edge Panel Thermo-Mechanical Analysis for Entry Conditions. In Proceedings of the 51st AIAA/ASME/ASCE/AHS/ASC Structures, Structural Dynamics, and Materials Conference, Orlando, FL, USA, 12–15 April 2010.
149. Singh, M.; Shpargel, T.P.; Morscher, G.N.; Asthana, R. Active Metal Brazing and Characterization of Brazed Joints in Titanium to Carbon-Carbon Composites. *Mater. Sci. Eng. A* **2005**, *412*, 123–128. [CrossRef]
150. Fu, Q.; Zhang, P.; Zhuang, L.; Zhou, L.; Zhang, J.; Wang, J.; Hou, X.; Riedel, R.; Li, H. Micro/Nano Multiscale Reinforcing Strategies toward Extreme High-Temperature Applications: Take Carbon/Carbon Composites and Their Coatings as the Examples. *J. Mater. Sci. Technol.* **2021**, *96*, 31–68. [CrossRef]
151. Ferro, D.; Rau, J.V.; Rossi Albertini, V.; Generosi, A.; Teghil, R.; Barinov, S.M. Pulsed Laser Deposited Hard TiC, ZrC, HfC and TaC Films on Titanium: Hardness and an Energy-Dispersive X-Ray Diffraction Study. *Surf. Coat. Technol.* **2008**, *202*, 1455–1461. [CrossRef]
152. Katoh, Y.; Vasudevamurthy, G.; Nozawa, T.; Snead, L.L. Properties of Zirconium Carbide for Nuclear Fuel Applications. *J. Nucl. Mater.* **2013**, *441*, 718–742. [CrossRef]
153. Hackett, K.; Verhoef, S.; Cutler, R.A.; Shetty, D.K. Phase Constitution and Mechanical Properties of Carbides in the Ta-C System. *J. Am. Ceram. Soc.* **2009**, *92*, 2404–2407. [CrossRef]
154. Kuo, C.C.; Lin, Y.T.; Chan, A.; Chang, J.T. High Temperature Wear Behavior of Titanium Nitride Coating Deposited Using High Power Impulse Magnetron Sputtering. *Coatings* **2019**, *9*, 555. [CrossRef]
155. Harrison, R.W.; Lee, W.E. Processing and Properties of ZrC, ZrN and ZrCN Ceramics: A Review. *Adv. Appl. Ceram.* **2016**, *115*, 294–307. [CrossRef]

156. Lévy, F.; Hones, P.; Schmid, P.E.; Sanjinés, R.; Diserens, M.; Wiemer, C. Electronic States and Mechanical Properties in Transition Metal Nitrides. *Surf. Coat. Technol.* **1999**, *120–121*, 284–290. [CrossRef]
157. Fahrenholtz, W.G.; Wuchina, E.J.; Lee, W.E.; Zhou, Y. Ultra-High Temperature Ceramics: Materials for Extreme Environment Applications. 2014. Available online: https://content.e-bookshelf.de/media/reading/L-2867458-4c0ab7c11a.pdf (accessed on 27 April 2026).
158. Zimmermann, J.W.; Hilmas, G.E.; Fahrenholtz, W.G.; Monteverde, F.; Bellosi, A. Fabrication and Properties of Reactively Hot Pressed ZrB2–SiC Ceramics. *J. Eur. Ceram. Soc.* **2007**, *27*, 2729–2736. [CrossRef]
159. Lynam, A.; Romero, A.R.; Xu, F.; Wellman, R.W.; Hussain, T. Thermal Spraying of Ultra-High Temperature Ceramics: A Review on Processing Routes and Performance. *J. Therm. Spray Technol.* **2022**, *31*, 745–779. [CrossRef]
160. Anusha, K.; Chakrabarty, S.; Routara, B.C.; Kumar, N.; Guha, S. A Review on Advancements in HVOF Sprayed Coating of MCrAlX Nicocraly Innovations in Processing Performance Applications and High Temperature Durability. *Discov. Mater.* **2025**, *5*, 233. [CrossRef]
161. Elshalakany, A.B.; Osman, T.A.; Hoziefa, W.; Escuder, A.V.; Amigó, V. Comparative Study between High-Velocity Oxygen Fuel and Flame Spraying Using MCrAlY Coats on a 304 Stainless Steel Substrate. *J. Mater. Res. Technol.* **2019**, *8*, 4253–4263. [CrossRef]
162. Simunovic, K.; Havrlisan, S.; Saric, T.; Vukelic, D. Modeling and Optimization in Investigating Thermally Sprayed Ni-Based Self-Fluxing Alloy Coatings: A Review. *Materials* **2020**, *13*, 4584. [CrossRef] [PubMed]
163. Singh, L.; Chawla, V.; Grewal, J.S. A Review on Detonation Gun Sprayed Coatings. 2012. Available online: https://www.scirp.org/journal/paperinformation?paperid=21028 (accessed on 27 April 2026).
164. Rajasekaran, B.; Raman, S.G.S.; Joshi, S.V.; Sundararajan, G. Performance of Plasma Sprayed and Detonation Gun Sprayed Cu–Ni–In Coatings on Ti–6Al–4V under Plain Fatigue and Fretting Fatigue Loading. *Mater. Sci. Eng. A* **2008**, *479*, 83–92. [CrossRef]
165. Srikanth, A.; Thalib Basha, G.A.; Venkateshwarlu, M. A Brief Review on Cold Spray Coating Process. *Mater. Today Proc.* **2019**, *22*, 1390–1397. [CrossRef]
166. Ghelichi, R.; Guagliano, M. Coating by the Cold Spray Process: A State of the Art. *Frat. Ed Integrità Strutt.* **2009**, *3*, 30–44. [CrossRef]
167. Marzbanrad, B.; Toyserkani, E.; Jahed, H. Customization of Residual Stress Induced in Cold Spray Printing. *J. Mater. Process. Technol.* **2021**, *289*, 116928. [CrossRef]
168. Liu, Y.; Zhang, R.; Liu, S.; Zhao, J.; Tang, X.; Liu, Y. Multi-Functional Design of Ultra-High Temperature Ceramics Coatings. *J. Mater.* **2026**, *12*, 101127. [CrossRef]
169. Gan, Z.; Ng, H.W.; Devasenapathi, A. Deposition-Induced Residual Stresses in Plasma-Sprayed Coatings. *Surf. Coat. Technol.* **2004**, *187*, 307–319. [CrossRef]
170. Besmann, T.M.; Mclaughlin, J.C.; Lin, H.-T. Fabrication of Ceramic Composites: Forced CVI. *J. Nucl. Mater.* **1995**, *219*, 31–35. [CrossRef]
171. Venkatachalam, V.; Blem, S.; Gülhan, A.; Binner, J. Thermal Qualification of the UHTCMCs Produced Using RF-CVI Technique with VMK Facility at DLR. *J. Compos. Sci.* **2022**, *6*, 24. [CrossRef]
172. Hu, C.; Hong, W.; Xu, X.; Tang, S.; Du, S.; Cheng, H.M. Sandwich-Structured C/C-SiC Composites Fabricated by Electromagnetic-Coupling Chemical Vapor Infiltration. *Sci. Rep.* **2017**, *7*, 13120. [CrossRef]
173. Tong, Y.; Bai, S.; Liang, X.; Qin, Q.H.; Zhai, J. Reactive Melt Infiltration Fabrication of C/C-SiC Composite: Wetting and Infiltration. *Ceram. Int.* **2016**, *42*, 17174–17178. [CrossRef]
174. Poovathingal, S.; Stern, E.C.; Nompelis, I.; Schwartzentruber, T.E.; Candler, G.V. Nonequilibrium Flow through Porous Thermal Protection Materials, Part II: Oxidation and Pyrolysis. *J. Comput. Phys.* **2019**, *380*, 427–441. [CrossRef]
175. Haskins, J.; Barnhardt, M.; Stern, E.; Meurisse, J.; Borner, A.; Semeraro, F.; Amar, A.; Monk, J.; Bessire, B.; Feldman, J. Overview of Ablation Modeling at NASA. 2022. Available online: https://ntrs.nasa.gov/api/citations/20220016583/downloads/ablation_overview_presentation.pdf (accessed on 27 April 2026).
176. Schroeder, O.M.; Schulz, J.C.; Bellas-Chatzigeorgis, G.; Shrestha, P.; Palmer, G.; Brock, J.M.; Stern, E.C.; Candler, G.V. Ares: A Coupling Methodology for Ablation Modeling. In Proceedings of the AIAA SCITECH 2024 Forum, Orlando, FL, USA, 8–12 January 2024.
177. Chen, Y.-K.; Milos, F.S.; Gökçen, T. Validation of a Three-Dimensional Ablation and Thermal Response Simulation Code. In Proceedings of the 10th AIAA/ASME Joint Thermophysics and Heat Transfer Conference, Chicago, IL, USA, 28 June–1 July 2010. [CrossRef]
178. Schulz, J.; Bellas-Chatzigeorgis, G.; Stern, E.; Palmer, G. *Presentation Title Overview of the Material Response Code Icarus*; NASA: Washington, DC, USA, 2023.
179. Chen, Y.-K. Thermal Ablation Modeling for Silicate Materials. In Proceedings of the 54th AIAA Aerospace Sciences Meeting, San Diego, CA, USA, 4–8 January 2016.

180. Carnimeo, I.; Affinito, F.; Baroni, S.; Baseggio, O.; Bellentani, L.; Bertossa, R.; Delugas, P.D.; Ruffino, F.F.; Orlandini, S.; Spiga, F.; et al. Quantum ESPRESSO: One Further Step toward the Exascale. *J. Chem. Theory Comput.* **2023**, *19*, 6992–7006. [CrossRef] [PubMed]
181. Batzner, S.; Musaelian, A.; Sun, L.; Geiger, M.; Mailoa, J.P.; Kornbluth, M.; Molinari, N.; Smidt, T.E.; Kozinsky, B. E(3)-Equivariant Graph Neural Networks for Data-Efficient and Accurate Interatomic Potentials. *Nat. Commun.* **2022**, *13*, 2453. [CrossRef] [PubMed]
182. Gaston, D.; Newman, C.; Hansen, G.; Lebrun-Grandié, D. MOOSE: A Parallel Computational Framework for Coupled Systems of Nonlinear Equations. *Nucl. Eng. Des.* **2009**, *239*, 1768–1778. [CrossRef]
183. Wen, M.; Afshar, Y.; Elliott, R.S.; Tadmor, E.B. KLIFF: A Framework to Develop Physics-Based and Machine Learning Interatomic Potentials. *Comput. Phys. Commun.* **2022**, *272*, 108218. [CrossRef]
184. Zhou, J.; Zhan, J.; Liang, H.; Guo, Y.; Zhao, B.; Hao, L.; Zhang, T.; Jiang, B. Modeling for the Fabrication Process of a Φ1185 Mm C/C Composite Thermal Insulation Tube in an Isothermal Chemical Vapor Infiltration Reactor. *Coatings* **2024**, *14*, 756. [CrossRef]
185. Shinde, V.M.; Kamal, A.; Rajasekhar, B.V.; Devasia, R.; Sharma, K. Modeling of Industrial Isothermal Chemical Vapor Infiltration Process for C/SiC Structural Composites. *J. Am. Ceram. Soc.* **2025**, *108*, e20591. [CrossRef]
186. Zuo, H.; Ruan, F.; Wang, H.; Wang, H.; Wang, X.; Huang, Y.; Wang, R.; Zou, L.; Xu, Z.; Li, D. Advances in Ablation or Oxidation Mechanisms and Behaviors of Carbon Fiber-Reinforced Si-Based Composites. *Molecules* **2023**, *28*, 6022. [PubMed]
187. Swaminathan Gopalan, K.; Schmitt, S.; Borner, A. DSMC Simulation of Etch Pit Formation through Active Sites in Carbon Fiber Micro-Structures. In Proceedings of the Direct Simulation Monte Carlo (DSMC) Conference 2023, Santa Fe, NM, USA, 24–27 September 2023.
188. Ferguson, J.C.; Semeraro, F.; Borner, A.; Panerai, F.; Thornton, J.M.; Izquierdo, S.F.; Quintart, A.; Mansour, N.N. Recent Developments to the Porous Microstructure Analysis (PuMA) Software. 2024. Available online: https://ntrs.nasa.gov/api/citations/20240008003/downloads/PuMA_ICTMS_Ferguson.pdf (accessed on 27 April 2026).
189. Amar, A.J.; Brandon Oliver, A.; Kirk, B.S.; Salazar, G.; Droba, J. Overview of the Charring Ablator Response (CHAR) Code. In *Proceedings of the 46th AIAA Thermophysics Conference*; American Institute of Aeronautics and Astronautics Inc., AIAA: Reston, VA, USA, 2016.
190. Baurle, R.A.; White, J.A.; Drozda, T.G.; Norris, A.T. VULCAN-CFD Theory Manual: Ver. 7.2.0. 2022. Available online: https://vulcan-cfd.larc.nasa.gov/WebPage/Documentation/manual_theory.pdf (accessed on 27 April 2026).
191. Helm, C.M.; Martín, M.P. Large Eddy Simulation of Two Separated Hypersonic Shock/Turbulent Boundary Layer Interactions. *Phys. Rev. Fluids* **2022**, *7*, 074601. [CrossRef]
192. Cerminara, A.; Levin, D.; Theofilis, V. Susceptibility of Shock-Transitional-Boundary-Layer Interaction to Shock Oscillations in Hypersonic Flow. In Proceedings of the AIAA SCITECH 2024 Forum, Orlando, FL, USA, 8–12 January 2024. [CrossRef]
193. Nurhaniza, M.; Ariffin, M.K.A.; Ali, A.; Mustapha, F.; Noraini, A.W. Finite Element Analysis of Composites Materials for Aerospace Applications. *IOP Conf. Ser. Mater. Sci. Eng.* **2010**, *11*, 012010. [CrossRef]
194. Maclean, M.; Barnhardt, M.; Wright, M. Implicit Surface Boundary Conditions for Blowing, Equilibrium Composition, and Diffusion-Limited Oxidation. In Proceedings of the 48th AIAA Aerospace Sciences Meeting Including the New Horizons Forum and Aerospace Exposition, Orlando, FL, USA, 4–7 January 2010.
195. Thornton, J.M.; Meurisse, J.B.E.; Prabhu, D.K.; Borner, A.P.; Monk, J.D.; Mansour, N.N.; Cruden, B.A. Analysis of MSL/MEDLI Entry Data with Coupled CFD and Material Response. 2021. Available online: https://ntrs.nasa.gov/api/citations/20210018054/downloads/IPPWPoster.pdf (accessed on 27 April 2026).
196. Thornton, J.M.; Prabhu, D.K.; Meurisse, J.B.E.; Borner, A.P.; Monk, J.D.; Cruden, B.A. Coupling CFD and Material Response for Analysis of Mars Entry. 2022. Available online: https://ntrs.nasa.gov/citations/20220016438 (accessed on 27 April 2026).
197. Michelle, M. Main LALTesting_MLM_TFAWS2022_30aug22 Image Representation. 2022.
198. Drew Turbeville, F.; Broslawski, C.J.; Cheatwood, J.S. Progress on Quantitative Infrared Thermography at the NASA Langley Aerothermodynamic Laboratory. In Proceedings of the AIAA Aviation Forum and Ascend 2024, Las Vegas, NV, USA, 29 July–2 August 2024.
199. Brune, A.J. Arc-Jet Overview, Modeling, and Uncertainty for Hypersonic Material Environmental Test and Evaluation. 2024. Available online: https://ntrs.nasa.gov/api/citations/20240002129/downloads/240216%20Arc_Jet_Testing_Overview_v6_STRIVES.pdf (accessed on 27 April 2026).
200. Paz, A.; Orozco, G.A.; Korhonen, R.K.; García, J.J.; Mononen, M.E. Expediting Finite Element Analyses for Subject-specific Studies of Knee Osteoarthritis: A Literature Review. *Appl. Sci.* **2021**, *11*, 11440. [CrossRef]
201. Wang, Z.; Fang, G.; Jin, X.; Wang, B.; Meng, S. Oxidation Damage and Residual Mechanical Properties Analysis for Cf/ZrB2-SiC Composites in Thermo-Oxygen Environment. *Compos. Struct.* **2025**, *370*, 119358. [CrossRef]
202. Leanos, A.L.; Prabhakar, P. Experimental Investigation of Thermal Shock Effects on Carbon-Carbon Composites. *Compos. Struct.* **2015**, *132*, 372–383. [CrossRef]

203. Zahid, M.; Sharma, R.; Bhagat, A.R.; Karra, P. Image-Based Numerical Modeling for the Effective Thermo-Elastic Property of 4D Carbon/Carbon Composite at High Temperatures. *Compos. Struct.* **2021**, *267*, 113881. [CrossRef]
204. Meng, S.; Zhou, Y.; Xie, W.; Yi, F.; Du, S. Multiphysics Coupled Fluid/Thermal/Ablation Simulation of Carbon/Carbon Composites. *J. Spacecr. Rocket.* **2016**, *53*, 930–935. [CrossRef]
205. Wang, X.; Jiang, P.; Tang, Y.; Zhang, W.; Shi, S. Microstructure-Based Thermochemical Ablation Model of Carbon/Carbon-Fiber Composites. *Materials* **2022**, *15*, 5695. [CrossRef]
206. Thornton, J.M.; Prabhu, D.K.; Cruden, B.A.; Meurisse, J.B.E.; Borner, A.P. Analysis of Mars 2020 Entry with Coupled Material Response and CFD. 2019. Available online: https://ntrs.nasa.gov/citations/20230015869 (accessed on 27 April 2026).